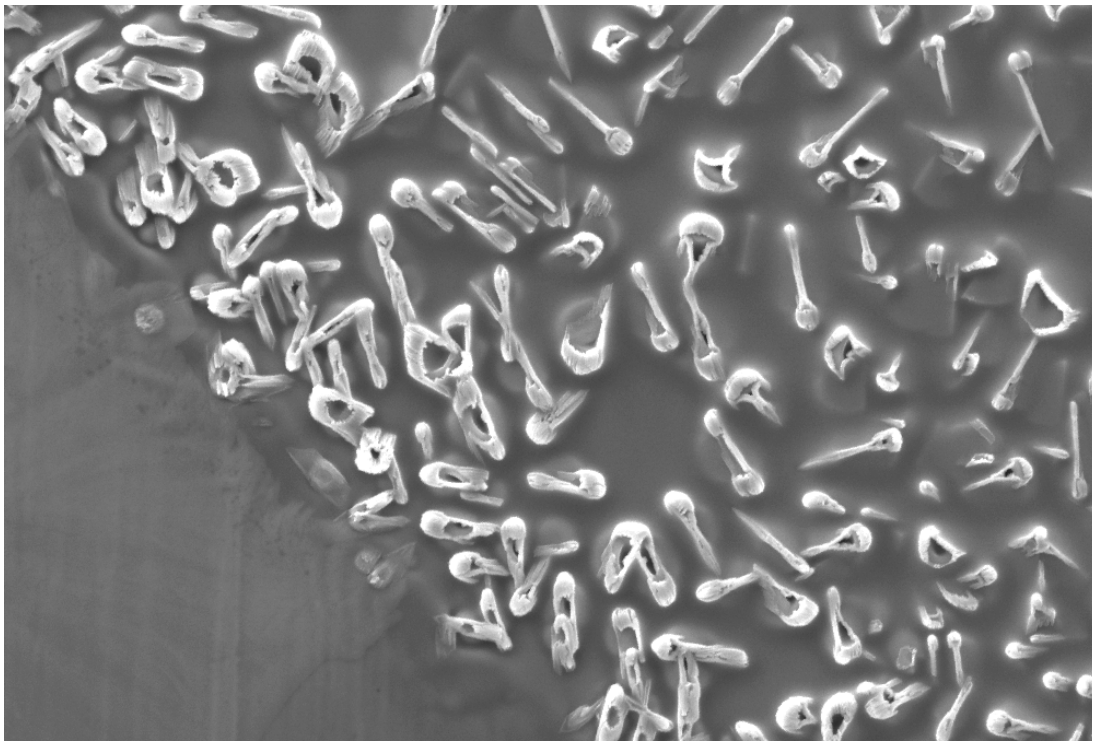
CHALMERS



Characterization of corrosion at bipolar plates in HTPEM fuel cells

Master of Science Thesis in the Master Degree Programme, Materials Chemistry and Nanotechnology

JOHANNA EKBERG

Department of Chemical and Biological Engineering
Division of Environmental Inorganic Chemistry
CHALMERS UNIVERSITY OF TECHNOLOGY
Gothenburg, Sweden, 2013

Characterization of the corrosion at bipolar plates in HTPEM fuel cells

J. EKBERG

Department of Chemical and Biological Engineering
CHALMERS UNIVERSITY OF TECHNOLOGY
Göteborg, Sweden 2013

Characterization of corrosion at bipolar plates in HTPEM fuel cells
J. EKBERG

© J. EKBERG, 2013.

Department of Chemical and Biological Engineering
Chalmers University of Technology
SE-412 96 Göteborg
Sweden
Telephone + 46 (0)31-772 1000

Supervisors: Jan Grolig & Patrik Alnegren
Examiner: Jan-Erik Svensson

Cover: [A SEM image of a 316L sample exposed to 25 % humidity and H_2/Ar gas at 180 °C for 168 hours. The image is taken at a magnification of 1000 times.]

Göteborg, Sweden 2013

Abstract

In electrical cars it is hard to predict the driving range when the battery is used for both driving the car and the auxiliary systems. This can be solved by combining the battery with a stack of HTPEM (high temperature polymer electrolyte membrane) fuel cells that can supply the auxiliary systems with electricity. The weight of the HTPEM stack is mostly due to the bipolar plate component. To achieve more lightweight fuel cells, bipolar plates made of stainless steel can be used instead of conventional graphite bipolar plates. The drawback with bipolar plates made of metal is a potentially higher degradation rate due to corrosion.

The corrosion performance of stainless steel 316L was investigated with furnace exposures in different environments. The experimental matrix was mimicking the fuel cell both in an active performance and in an inactive off mode, and simulated both the anode side and the cathode side. The atmosphere was controlled and the gas flow, type of gas, exposure time, temperature and humidity was alternated to arrange these different experimental conditions. Also Max Phase coated stainless steel 316L was tested in order to investigate its performance as a protective coating.

The exposure in cathodic atmosphere at 180 °C and 25 % humidity seemed to cause the highest oxidation rate. This exposure had the highest mass gain and the largest leaching of ions in the water during cleaning after exposure. The corrosion product formed on the samples during cathodic environment exposure was $FeH_yP_2O_7$ and the corrosion product formed on the samples exposed to an anodic environment was $FeH_2P_2O_7$.

Keywords: Oxidation, corrosion, fuel cells, HTPEM, phosphoric acid, stainless steel, corrosion, bipolar plates.

List of acronyms and abbreviations

CAS	Chemical abstract service
EDX	Energy disperse X-ray
HTPEM	High temperature polymer electrolyte membrane
HOMO	Highest occupied molecular orbital
ICP-AES	Inductively coupled plasma atomic emission spectrometry
LUMO	Lowest unoccupied molecular orbital
MP	Max Phase
PBI	Polybenzimidazole
SEM	Scanning electron microscopy
TPB	Triple phase boundary
XRD	X-ray diffraction

Acknowledgements

Thanks to my supervisors Patrik Alnegren and Jan Grolig for support and positive minds, my examiner Jan-Erik Svensson for the possibility to write this master thesis, Esa Väänänen for making electrodes, Charlotte Bouveng for her helpfulness and Jan Froitzheim for introducing me to the subject and the fuel cell group. Last, thanks to my classmates, I would never managed this far without you.

Table of contents

Abstract *iv*
List of acronyms and abbreviations *vi*
Acknowledgements *vi*
Table of contents *vii*
1. Introduction *1*
1.1 Background 1
1.2 Purpose 1
1.3 Problem and Task 1
1.4 Limitations 2
2. Theoretical background *3*
2.1 Fuel cells 3
2.2 Oxidation theory 4
2.3 Forms of corrosion 7
2.4 Material choice for the bipolar plates 8
2.5 Phosphoric acid, H_3PO_4 9
2.6 Characterization methods 10
3. Experimental *13*
3.1 Material 13
3.2 Sample preparation 13
3.3 Contact angle 16
3.4 Photography and Microscopy 16
3.5 XRD 16
3.6 SEM 16
3.7 Resistance measurement 16
3.8 ICP-AES 17
4. Results *18*
4.1 Contact angle 18
4.2 Photography and Microscopy 18
4.3 XRD to examine the corrosion products 21
4.4 SEM-EDX to examine the corrosion products 22
4.5 Mass change for quantification of corrosion 23
4.6 Resistance for quantification of corrosion 24
4.7 ICP-AES for quantification of corrosion 25
4.8 Inconel 625 26
5. Discussion *28*
5.1 Corrosion product 28
5.2 Quantification of corrosion 29
5.3 Parameters 30
5.4 Inconel 625 32
6. Conclusion *33*
7. Future outlook *33*
8. References *34*

1. Introduction

1.1 Background

In electrical cars batteries are used for supplying the car with energy for both driving the car, but also for temperature regulation systems, the computer and other auxiliary systems. The use of auxiliary systems will compromise the driving range of the vehicle to different extents depending on the use. This can cause inconvenience for the user, especially during winter, since the driving range will fluctuate and will be hard to predict. A current project aims to solve this issue by combining the battery with a HTPEM (high temperature polymer electrolyte membrane) fuel cell stack, which supplies electricity to the auxiliary systems.

A HTPEM fuel cell converts the energy of hydrogen directly into electrical energy, there will be no burning of fuel compared to a combustion engine driven generator [1]. The emissions will therefore be lower; no emissions of NOx and only low emissions of CO_2 [2]. This makes the fuel cell an environmental friendly energy source [1]. HTPEM fuel cells use hydrogen and oxygen as fuel and the output consist of mainly water [3]. The production of hydrogen is the part of the process that can affect the environment negatively and a lot of research is required before pure hydrogen is available as fuel for consumers [4]. In this project the hydrogen will come from reformed diesel, ethanol or gasoline: fuels that are available at gas stations. The use of reformed fuel, instead of pure hydrogen, creates some CO_2 emission.

Fuel cell stacks consist of several fuel cell elements, which are connected by bipolar plates that collect and conduct current from cell to cell and separate the gases [1]. Bipolar plates are the component in HTPEM fuel cells that have the highest impact on the weight and volume of a stack [1]. The bipolar plates that are most commonly used are made of graphite due to its corrosion resistance and high electrical conductivity [1]. There are though some disadvantages with graphite, it is expensive, needs machining, has low mechanical strength and makes a heavy stack due to the thickness [1]. To achieve a lighter stack stainless steel may be used. Stainless steel has good heat and electrical conductivity and can be thin because of its non-porosity that effectively will keep the gases apart [1]. A problem with stainless steel in the HTPEM fuel cells is the risk for corrosion. To avoid corrosion the stainless steel will most likely need to be coated.

1.2 Purpose

The purpose of the thesis is to investigate the corrosion performance at bipolar plate material made of stainless steel after certain furnace exposure in different environments. Both uncoated and coated stainless steel will be analysed. A method for quantification of the corrosion, and also a characterization method for investigation of the corrosion product, will be chosen and developed.

1.3 Problem and Task

The problem in a HTPEM fuel cell is the migration of phosphoric acid from the membrane towards the bipolar plates. The phosphoric acid accelerates oxidation and this can cause metal ions to diffuse into the membrane [5][6]. The metal ions might exchange with the membrane protons causing the resistance in the membrane to increase and lower the capacity of the fuel cell [6]. Of more importance is that the accelerated oxidation can cause a less efficient fuel cell due to a lower conductivity through the bipolar plate since the oxide layer has a higher resistance than an unoxidized metal [7].

The task is to investigate the corrosion at samples exposed to phosphoric acid during furnace experiments performed with different exposure times, water contents, atmospheres and temperatures. It is of interest to find the most aggressive environment, with respect to oxidation, when using stainless steel as bipolar plates in a fuel cell.

The corrosion will be analysed by several different methods, light microscopy, X-ray diffraction (XRD), scanning electron microscopy (SEM) with energy disperse X-ray (EDX), mass change, resistance measurements and inductively coupled plasma atomic emission spectrometry (ICP-AES).

1.4 Limitations

The results will not show the full picture about the actual performance of the stainless steel chosen as bipolar plates in a HTPEM fuel cell, electrical properties are of big concern as well. Experimental atmospheres aims to replicate the environment of a real HTPEM fuel cell stack, but in order to fully evaluate the relevance of the experimental setup, comparison to bipolar plates exposed in real stacks has to be made, which is out of scope for this thesis.

2. Theoretical background

2.1 Fuel cells

There are different types of fuel cells, they can be classified in temperature range or electrolyte used [8]. All of them operate with the same principles; they convert the chemical energy of fuel directly into electrical energy [3]. Fuel cells use hydrogen and oxygen as fuel and produce electrical energy [9]. A fuel cell is in it self completely CO_2-emission free when using pure hydrogen as fuel, but the production of hydrogen fuel can cause emissions. In the current project the hydrogen is supplied from reformed diesel, ethanol or gasoline, which causes some CO_2 emissions.

In this report the focus is on the HTPEM fuel cell. HTPEM is the fuel cell type that is most suited for transport applications [6]. They differ from other fuel cells by having a phosphoric acid doped PBI (polybenzimidazole) membrane as electrolyte [6]. This fuel cell can handle some impurities, 1 % of CO in the fuel will lead to minor loss of power density compared to the use of pure hydrogen [6]. This tolerant behaviour makes the HTPEM fuel cell usable with hydrogen produced from reformed fuels.

A fuel cell can be divided into two parts separated by a membrane. One part consists of a bipolar plate, the anode, and a catalytic surface, and the other part of a bipolar plate, the cathode and a catalytic surface [10]. The bipolar plates collect and conduct current from one fuel cell in a stack to another by connecting the anode of one cell with the cathode of an other [1]. The bipolar plates also separate gases in adjacent cells and provide structural support for the stack [1]. The electrodes conduct electrons that are released in the anodic reaction and complete the electrical circuit [1]. The catalyst surface is in close contact with the membrane and is the area where the electrochemical reactions take place [1]. The PBI-membrane has to be proton conductive but electronic insulating, and is doped with phosphoric acid to improve the proton conductivity. Figure 1 shows an illustration of a fuel cell in cross-section.

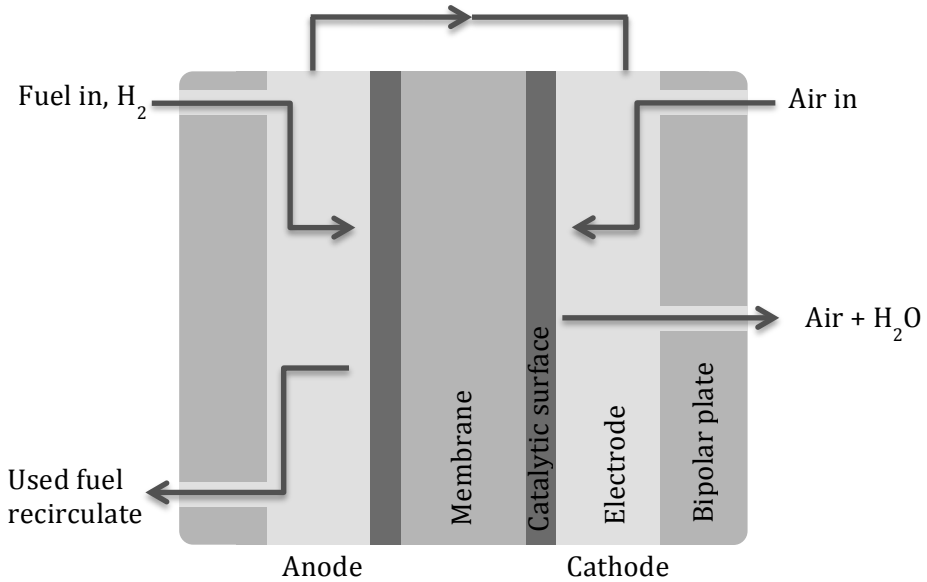


Figure 1. Cross-section of a fuel cell. Illustration of the conversion from fuel into electricity.

The reactant, hydrogen, is delivered to the anodic side and the oxidant, oxygen, to the cathodic side of the fuel cell. The transport is efficiently done due to the flow field plates, the bipolar

plates, that contain many fine channels that carry the gas flow and distribute the gas evenly at the surface [1]. The electrochemical reactions occur at the catalytic surface [10]. The reactions can only occur at defined sites where electrolyte, gas, and catalytic particles are in contact [11]. These defined sites are called TPB, triple phase boundaries. Fast electrochemical reactions result in a high current output and an enhanced performance of the fuel cell, so it is of importance to have the right kinetics and choose a suitable catalyst [10]. A fast electrochemical reaction occurs where the TPB sites are optimized, where the contact between the three phases are optimal [11].

The reactions in a fuel cell happen simultaneously at the anode and cathode. At the anode the supplied hydrogen molecules are splitted, electrons are released, and hydrogen ions formed, see equation 1. The hydrogen ions are diffusing through the proton conducting membrane and the electrons are traveling in the external circuit to the cathode [10]. At the cathode the reaction between the hydrogen ions from the anode and the oxygen supplied from the air is reacting on the catalyst surface and water is produced, see equation 2 [9]. Equation 3 is the net reaction in a fuel cell [9]. The transfer of electrons in the external circuit creates electricity due to the potential difference created by the two electrode reactions [8].

$$H_2 \leftrightarrow 2H^+ + 2e^- \quad (1)$$

$$\frac{1}{2}O_2 + 2H^+ + 2e^- \leftrightarrow H_2O \quad (2)$$

$$H_2 + \frac{1}{2}O_2 \leftrightarrow H_2O \quad (3)$$

2.2 Oxidation theory

There are different types of corrosion, atmospheric corrosion is one of them and occurs when there is an electrolyte present and in uncontrolled environments where rain, atmospheric impurities, sunlight, changes in humidity and temperature affects the corrosion [12]. In HTPEM fuel cells the temperature is relatively low and atmospheric corrosion occurs. Atmospheric corrosion on metals is an electrochemical process [13].

2.2.1 Corrosion process

Corrosion can be defined as the process where a metal reacts with its environment to form an oxide [12]. For corrosion to occur there need to exist two electrodes, a cathodic and an anodic, and one electrolyte. The distribution of anodic and cathodic areas determines the type of corrosion behaviour. For general, uniform corrosion the areas are distributed randomly over the metal and the reactions typically equation 4, 5 and 6 [12].

$M \rightarrow M^{n+} + ne^-$ Anodic reaction (4)

$O_2 + 2H_2O + 4e^- \rightarrow 4OH^-$ Cathodic reaction (5)

In environments with low pH the cathodic reaction may occur with hydrogen evolution instead.

$2H^+ + 2e^- \rightarrow H_2$ Cathodic reaction (6)

The second law of thermodynamics, Gibbs free energy, tells if an oxidation reaction is thermodynamically possible or not. If Gibbs free energy is smaller than zero, the metal will oxidize. The equation can, for constant temperature and pressure, be written as

$$\Delta G = \Delta H - T\Delta S \quad (7)$$

where ΔH is the change in enthalpy in $\mathrm{J/mole}$, T is the temperature in Kelvin and ΔS is the change in entropy in $\mathrm{J/mole \cdot K}$.

For electrochemical reactions the Gibbs free energy can also be calculated from

$$\Delta G = -nFE \quad (8)$$

where n is the number of electrons transferred in respective reactions, F is Faraday´s constant and E is the cell potential [14] [15]. Corrosion will occur if ΔG is negative, i.e. when the cell potential is positive. The cell potential is the difference in the two half-cell reactions, the one at the cathode subtracted from the one at the anode. When a metal is corroding, both the anodic and the cathodic half-cell reactions occur simultaneously at the electrochemically conductive surface [15].

Every material exposed to the atmosphere has a thin layer of water on the surface. The thickness of the water layer will depend on the relative humidity and the temperature [14]. This liquid may serve as an electrolyte where the electrochemical reactions can occur and oxygen can easily be transferred in the water film during atmospheric corrosion. Relative humidity and temperature depend on each other [16]. At constant relative humidity an increase in temperature will increase the corrosion [16]. If the humidity varies an increase in temperature lead to a lower relative humidity and the electrolyte on the material surface will evaporate faster and the corrosion rate will therefore be reduced [16]. An increase in temperature tends to increase the amount of corrosion, because electrochemical reactions and diffusion processes will increase with temperature [16].

2.2.2 Passivity

A thin protective oxide layer will often be formed at the metals and act corrosion resistance and is of importance to protect the metal from failure; a passive oxide layer [17]. The properties of the passive oxide layer will determine how resistant the metal will be against degradation. A passive oxide layer should be continuous, adherent, thin and slow growing and is formed by adsorption of oxygen onto the metal surface [15] [18]. The formation of an oxide layer starts by the formation of oxide islands on the metal surface [19]. The layer of oxygen atoms and formed oxide islands separates the metal from the oxygen in the atmosphere. Further corrosion is now limited by ions diffusing through the oxide layer, which significantly decreases the corrosion rate [18]. At higher temperatures the thermal energy is used for ions to overcome the energy barrier for diffusion, but due to the low temperature in the present study there is less thermal energy, therefore the quantum mechanical concept of electron tunnelling occurring instead [19]. The tunnelling of electrons generate an electric field across the oxide and the field makes the oxide layer grow more easily due to a lowering of the activation energy for ion movement [19]. See figure 2 that illustrates the oxide layer growth.

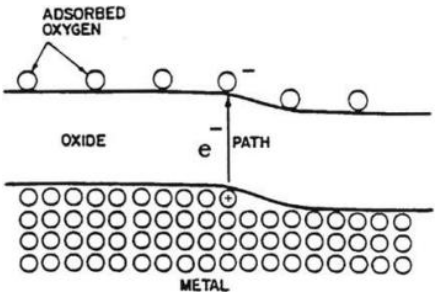


Figure 2. How the oxide layer is growing at low temperature with an electrolyte present [18].

2.2.3 Passivity breakdown

When the temperature is raised, and the relative humidity increased, the oxidation continues and the protection from the passive oxide layer may failure [18]. The continuing oxidation mechanism may lead to degradation of the metal.

2.2.4 Kinetics

There is one rate law that is most commonly occurring for the formation of the passive layer for atmospheric corrosion, the logarithmic rate law, see figure 3 [19]. Logarithmic rate law can for atmospheric oxidation be either inverse or direct [19]. At intermediate temperature, logarithmic kinetics for atmospheric oxidation may after some time transform into parabolic kinetics [19]. The parabolic kinetics means that the oxidation rate is inversely proportional to the square root of time [18]. The rate laws are illustrated in figure 3, with weight gain versus time. It can be seen that the oxidation rate decreases when the oxide layer grows thicker due to a thicker diffusion path, i.e. the rate laws are diffusion controlled [18]. The rate laws are of interest to achieve information about the dominating mechanism during oxidation and also predict the forthcoming oxidation.

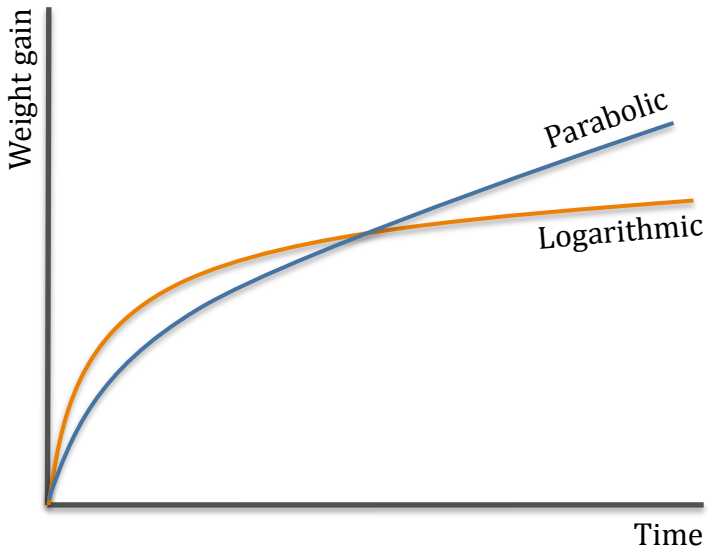


Figure 3. Weight gain versus time. The two kinetic rate laws for metal oxidation at atmospheric corrosion. Figure inspired by Jones, D.A. Principles and prevention of corrosion [15].

2.3 Forms of corrosion

There are different types of corrosion mechanisms, they can occur alone or in company with other types of corrosion. Some examples of mechanism that are of interest during current project are uniform corrosion, galvanic corrosion, intergranular corrosion, crevice corrosion and pitting corrosion. [15]

2.3.1 Uniform corrosion

Uniform corrosion is considered as the simplest form of corrosion, it is predictable and it proceeds at approximately the same rate at the complete surface. Uniform corrosion is distributed over the entire surface of a metal, but to occur the corrosive environment has to have the same access to the complete surface. [14][15]

2.3.2 Galvanic corrosion

Galvanic corrosion occurs when two different metals in a conductive solution are electrically connected and one of them corrodes and the other one is protected. Any metal will preferentially corrode if it is connected to a metal that is nobler in the Galvanic series. The galvanic series for metals gives information about how the galvanic current will flow between two metals in contact and which one that will corrode. [14][15]

2.3.3 Intergranular corrosion

Intergranular corrosion take place in the grain boundaries of a metal and can happen when the grain boundaries becomes depleted of passivation elements. The grain boundary will act as the anode and the rest of the metal as the cathode. The small size of the anode compared to the larger cathode will cause a rapid attack that will penetrate deep into the metal. [14][15]

2.3.4 Crevice corrosion

Crevice corrosion takes place in narrow sheltered areas as a result of differences in oxygen concentrations, crevices where liquid can get stagnant, lap joints or deposits on the metal surface. The narrow gap or opening can be formed by metal-metal or metal connected to other materials. If two different metals make up the crevice it can be companied by galvanic corrosion. [14][15]

2.3.5 Pitting corrosion

Pitting corrosion is a localized attack on a surface that otherwise is resistant to corrosion. Pitting is relatively rapid corrosion that creates holes or pits. Initiation of the pit is associated with the breakdown of the protective film, oxide layer or coating on a metal surface. The breakdown can be due to defects in the protective film, such as soil, irregularities in the morphology of the metal, bad adhesion of the coating or an acidic environment. When corrosion occurs at this small area the pit gets a lack of oxygen and will become a localized anode due to change in potential. The large surrounding area then becomes the cathode. With a small anode in comparison to a large cathode the anodic current density will be high and rapid corrosion will occur. The pit makes a sheltered location where corrosion can propagate down in the metal and create deeper pits and then finally destroy the material. [14][15]

2.4 Material choice for the bipolar plates

The most common type of material used for bipolar plates is graphite-based material. Graphite is suitable due to its good electrical conductivity and its chemical stability in the corrosive fuel cell environment but the permeability is high, so a bipolar plate made up by graphite need to be thick to not let gases diffuse through. The necessary thickness of the bipolar plates leads to a large and heavy stack.

Instead of graphite metal may be used as bipolar plate material. Metals can be relatively thin without letting gases diffuse through, due to very low permeability [4]. This will lead to a light stack. Metals have a higher mechanical strength and a better durability to shock and vibration compared to graphite [20]. The drawback with metals is oxidation, which can lead to two problems. Ions can diffuse in to the membrane and exchange with protons and thereby lowering the conductivity and increase the resistance [6]. The other important concern is that the oxide layer has lower conductivity than the metal itself, which may lead to an increased contact resistance after oxidation [6]. Oxidation of the bipolar plates can thereby lower the capacity of the fuel cells.

In this thesis stainless steel 316L is chosen as metallic candidate and have been tested in terms of its suitability to be used as bipolar plate material. Stainless steel 316L has also been tested with a protective coating, a Max Phase coating, to examine if a coating leads to a better protection against corrosion. Another metal is compared to stainless steel 316L, nickel-chromium alloy Inconel 625, this to consider a more corrosion resistant metal as bipolar plate.

2.4.1 Stainless steel 316L

Stainless steel 316L is the low carbon version of type 316, the L stands for low carbon. 316L is an austenitic stainless steel with a Cr/Fe ratio of 0.25 [21]. The higher Cr/Fe ratio the better is the corrosion resistance [21]. The composition of stainless steel 316L can be seen in table 1.

2.4.2 Inconel 625

Inconel 625 is a nickel chromium alloy and has a much higher Cr/Fe ratio than 316L, 4.40, and is then more resistant to corrosion [21]. Another factor that affects the corrosion resistance is the amount of nickel. Inconel 625 consist of 58 wt% nickel compared to 12 wt% nickel in 316L. Nickel is corrosion resistant by itself and as alloy [22]. Nickel stabilizes the austenite face centred cubic phase during corrosion, which cause good creep resistance [15].

Table 1. The composition of stainless steel 316L and Inconel 625 in weight percentage. [21]

wt%	**Fe**	**Cr**	**Ni**	**Mn**	**Si**	**Mo**
316L	67	17	12	1.0	0.4	2.5
625	5.0	22	58	0.5	0.5	9.0

2.4.3 Max Phase

The Max Phase coating supplied for this project has an unknown composition, but Max Phase in general is known as hexagonal nitrides or carbides. Max Phase has the general formula

$$M_{n+1}AX_n \tag{9}$$

where $n = 1 - 3$, M is an early transition metal, A is an A-group element and X is either a carbon and/or a nitrogen atom. The A-group elements got this name after the old CAS nomenclature (chemical abstract service nomenclature) where the A-group corresponded to the main group elements, the elements from group 1-2 and 13-18 in the periodic table (except hydrogen). In figure 4A the elements that are already discovered combined into a Max Phase compound are marked with a colour. The early transition metals are marked red, the A-group elements blue and X is marked in black. [20][23]

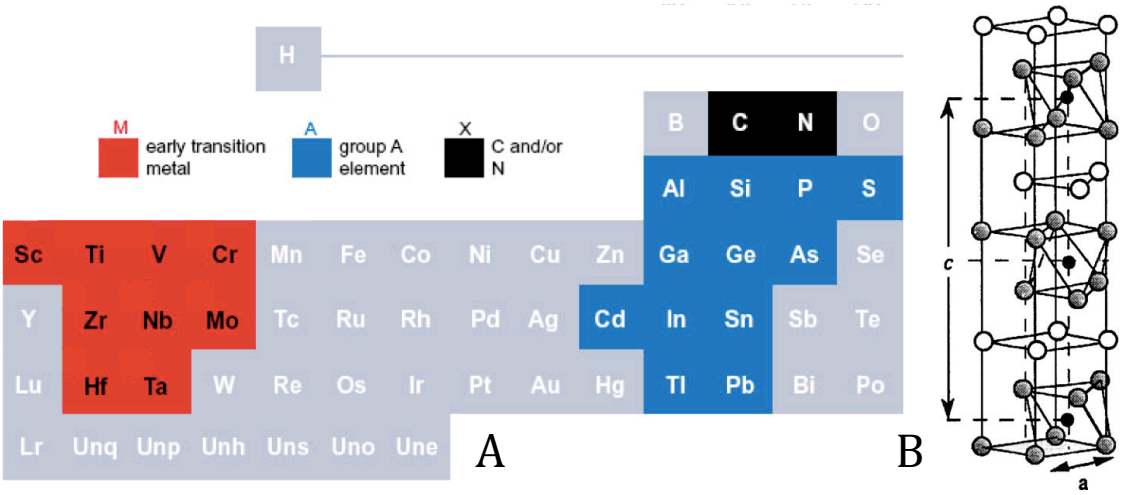


Figure 4. A) Elements that are discovered in a Max Phase compounds are marked red, blue and black. The red elements are at the left, the blue at the right and the black on top of the blue elements. Figure inspired by Department of Material Science and Engineering at Drexel University. MAX Phases. [24]. B) The structure of M_2AX_1. M is grey, A is white and X is black [25].

These carbides and nitrides have good physical, electrical, chemical and mechanical properties. They exhibit the behaviour of a metal and a ceramic material at the same time; they collected the best properties from both. They conduct heat and electricity, are damage tolerant, are plastic at high temperatures and are almost as machinable as a metal. They are elastically rigid, strong, brittle and lightweight like ceramics. Some of the Max Phase compounds (for example Ti_3SiC_2 and Ti_2AlC) are resistant to creep, corrosion and oxidation. The MX layers are twinned with respect to each other and separated by the A layer that acts as a mirror plane. The Max Phase has the X-ion in the centre of the M-octahedron. See figure 4B. [20][23]

2.5 Phosphoric acid, H_3PO_4

The PBI-membrane in a fuel cell is doped in phosphoric acid to achieve good proton conduction for the hydrogen ions to diffuse from the anodic side of the fuel cell to the cathodic side, and thereby achieve good capacity of the fuel cell. The drawback with phosphoric acid is the possible migration of acid from the membrane towards the bipolar plates. Phosphoric acid may accelerate oxidation of the stainless steel bipolar plates [5]. Pure phosphoric acid is a colourless crystalline material that are soluble in water and has a density of 1.88 g/cm^3 and a melting point of 42.35 °C [26]. Phosphoric acid with 85 % concentration has the colour in-between transparent and off-white and has a high viscosity. The composition of concentrated phosphoric acid is a function of the phosphorus pentoxide, P_2O_5, content [27]. When phosphoric acid is getting more concentrated the concentration of phosphorus pentoxide content increases as well [26]. See equation 10 where M is the molar mass [28].

$$wt\%\ H_3PO_4 = 2\frac{M_{H_3PO_4}}{M_{P_2O_5}} \cdot wt\%\ P_2O_5 \quad (10)$$

Concentrating of phosphoric acid does not happen spontaneously, phosphoric acid is hygroscopic and striding towards maintaining the equilibrium [27]. Equation 11 shows the reaction with phosphoric acid and phosphorus pentoxide [28]. The equilibrium of this reaction is preferably towards phosphoric acid [28].

$$2 \cdot P_2O_5 + 6 \cdot H_2O \leftrightarrow 4 \cdot H_3PO_4 \quad (11)$$

2.6 Characterization methods

There were three methods used for analysing the corrosion product on the exposed samples, light microscopy, SEM with EDX and for the crystalline products; XRD. There were four methods used for quantifying the corrosion of the exposed samples, mass change, resistance measurement, ICP-EAS and microscopy. Resistance was used to give a value of the change in resistance due to the thickness of the oxide layer. ICP-EAS was usable to quantify the ions in the water collected from the cleaning process of the exposed samples.

2.6.1 X-ray diffraction

X-ray diffraction, XRD, is a technique used for analysis of solid crystalline samples. It is a miscellaneous technique that gives crystallographic information that can be compared to a database with standards. This crystallographic information can give the chemical composition of the crystalline phase. The XRD instrumentation radiates monochromatic X-rays with wavelength lambda, λ, and an incident angle theta, θ, towards a crystalline sample. These X-rays will interact with the crystals in the sample and scatter due to the three-dimensional symmetry of the unit cell. The directions of the scattered beams are a function of the wavelength of the radiation and the specific interatomic spacing, d_{hkl}, of the plane in the unit cell from which the radiation occurs. In some directions an increased intensity can be observed due to constructive interference of the scattered waves. Constructive interference will be observed when Braggs law is valid, equation 12. The interference pattern is specific for each substance.

$$n\lambda = 2d_{hkl}\,sin\,(\theta) \quad (12)$$

where n is an integer, λ is the wavelength of the incident wave, d_{hkl} is the spacing between the atomic planes and θ is the angle between the incident X-ray and the atomic plane. Figure 5 illustrates Braggs Law with incoming waves with a specific wavelength interacting with crystals in a set of atomic planes. [29]

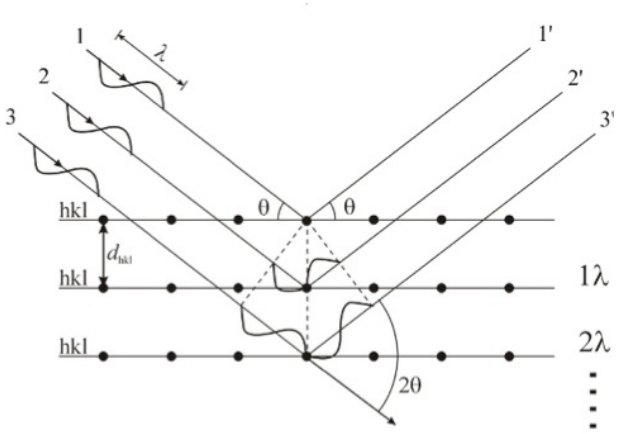


Figure 5. A set of crystal planes with the spacing d_{hkl}, and the angle θ between the incoming X-rays and the crystal plane. The incoming X-ray has the wavelength λ. [30]

2.6.2 Scanning electron microscopy

Scanning electron microscopy, SEM, is a microscopic method that utilizes the generation of signals from an electron beam that have swept over a solid surface. The interactions between electrons with high kinetic energy and a solid surface give rise of signals that provide information about the compounds morphology, the chemical composition, its crystal structure and the orientation of materials.

The samples are placed in a vacuum chamber after being prepared to conduct electricity. An electron gun accelerates electrons towards the sample and magnetic lenses compact the electron beam to achieve a fine focus. When the electron beam interacts with the surface it excites electrons from the top layers and some of the electrons escape and are detected. There are two types of electrons that are deflected from the surface, inelastic and elastic electrons. The inelastic electrons, also called the secondary electrons, are low-energy particles that are caused by topography and surface variations. The elastic electrons are the high-energy electrons, also called the backscattered electrons. Their collision with the surface produces specific energy quanta and they can give information about the crystal structure, the sample composition and the elements and chemicals present in the different layers of the surface. [31]

EDX is used in combination with SEM. An EDX detector makes it possible to get an additional image of the sample by observing the X-ray emission caused by the electron beam. The emission spectrum is specific for each substance and will contribute with information about the sample elements. With EDX it may be possible to identify the composition of the sample and showing the element distribution on the surface. [32]

2.6.3 Electrical resistance

Resistance, R, is a measurement of the limiting factor for a current to flow through an electrical circuit when an electrical potential is applied [33]. A metal is electrically conductive due to free moving electrons in the material [33]. The strength of the electric conductivity is due to the amount of free moving electrons and the amount of positive ions that collide and retarding the electrons on their way towards the positive pole. The higher value the resistance have, the higher is the limiting factor and a higher voltage is needed to force a specific current through a circuit. The resistance is measured in ohm and can be calculated with Ohms law, equation 13.

$$R = {}^{U}/_{I} \tag{13}$$

where R the resistance, U is the voltage and I the current [33].

The resistance could be used as a method to characterize the corrosion that occurs at the samples in this project. When a metal oxidize an oxide layer is formed. The oxide layer has a lower conductivity than the metal, due to larger band gap between HOMO and LUMO that prevents motion of the free electrons between the valence band and the conduction band [34]. A thicker oxide layer leads to a higher resistance for the current to flow through the sample [7]. The resistance can be used to quantify the corrosion due to linearity for the oxide thickness and the resistance. The resistance can be a value of the overall performance of bipolar plates in fuel cells.

2.6.4 Inductively coupled plasma emission spectrometry

Inductively coupled plasma atom emission spectrometry, ICP-AES, is an analytical method used for determining the concentration of water-soluble ions in a solution. The instrument uses argon plasma in which the ions in the sample-solution immediately collide with the ions and electrons in the plasma and also with itself. Some of the atoms in the sample have then excited to a higher state and when they return to the ground state they emit radiation with the characteristic wavelengths of the elements involved. The emission intensity is proportional to the concentration of the elements within the sample. To get the concentration of a specific element in the sample a calibration curve is needed, the calibration curve need to consist of all the elements of interest and the concentrations are calculated by interpolation. [35]

3. Experimental

The experiments are an approach to simulate the environment for a bipolar plate in a HTPEM fuel cell. The experimental matrix was aimed to mimic the fuel cell both in an active performance and a passive off mode, and the bipolar plate at both the anode side and the cathode side. The atmosphere was controlled and the gas flow, type of gas, exposure time, temperature and humidity was alternated to arrange these different experimental setups. The stainless steel used as bipolar plate material was sprayed with phosphoric acid before furnace exposure to mimic the migration of phosphoric acid from the membrane in a HTPEM fuel cell.

3.1 Material

Stainless steel 316L was used and examined in different atmospheres to find the most corrosive environment during exposure. Stainless steel 316L coated with Max Phase was also exposed to investigate if a coating would protect the stainless steel during furnace exposures. In one experiment 316L was compared to nickel-chromium alloy Inconel 625 to see if the performance of Inconel 625 during furnace exposure is better, and in what way. The Max Phase coated steel was delivered from the Impact Coatings AB with a substrate thickness of 0.2 mm, and the Max Phase coating used in current project was made by placing the stainless steel on a net and coat it from both sides. The thickness of the stainless steel 316L sample was 0.1 mm for the room temperature exposure and 0.2 mm for the other exposures. Inconel 625 samples had a thickness of 0.2 mm.

3.2 Sample preparation

The preparation of the samples is a method that was developed during the first weeks of the experimental procedure and different ways of sample preparation were tested.

The samples were first cut with a large metal cutter to achieve the same size and fine edges. The samples were cut in different sizes, 15x15, 17x17 and 20x20 mm^2. The sample size was changed during the experimental procedure; a sample with a larger surface area achieves more correct corrosion quantification, with respect to mass change and appearance. In contrast, smaller samples allow more samples to fit into the tubular furnace at the same time and then a better statistic comparison can be performed with respect to reproducibility.

3.2.1 Cleaning before exposure

All the samples were cleaned in the same manner, using ultrasonic agitation. First in acetone for ten minutes at room temperature, then in ethanol for ten minutes at room temperature. Afterwards the samples were dried with compressed air. All the samples were then weighed with a Satorius MC 5 micro-balance two times and the average value was used for analysis.

3.2.2 Adding phosphoric acid

The clean samples were placed in a grip holder and sprayed, from a distance of 20 cm, with 5 M phosphoric acid, see figure 6. The samples were sprayed with four showers and let dry for one minute. This procedure was repeated four times or until all samples had a similar amount of phosphoric acid added, near 1.55 mg/cm^2. To achieve an even layer of phosphoric acid on the samples they were placed in a drying furnace at a temperature of 110-120 °C.

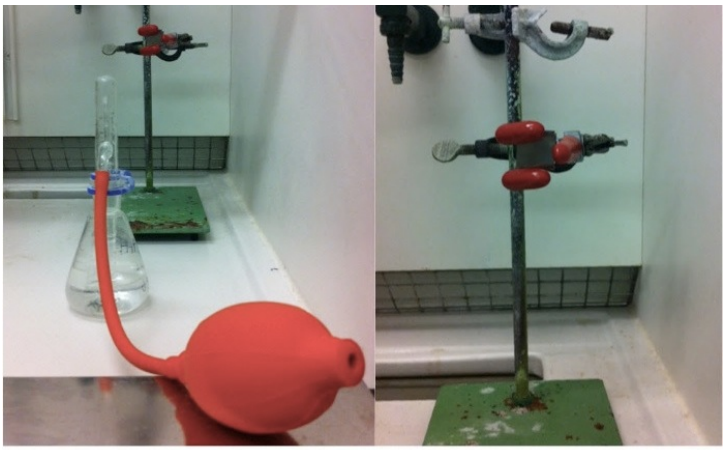


Figure 6. Spraying the samples with 5M phosphoric acid from 20cm distance.

3.2.3 Furnace exposure and test parameters

Horizontal tubular furnaces were used, see figure 8. One of the furnaces was fed with high water vapour and to avoid condensation the inlet tubing needed a high temperature at every point in the system. The dew point was calculated from table *Vapour pressure of water below 100 °C* in Data and Diagram [36]. A temperature profile was recorded over the furnace by measure the temperature every second centimetre by starting at the warmest area, close to the middle of the furnace, and moving outwards to both sides. A graph, figure 7, was made with temperature against position, with the warmest area of the furnace as position zero. The temperature tolerance was decided at +/- 5°C, which resulted in 10 cm of usable testing space inside the furnace.

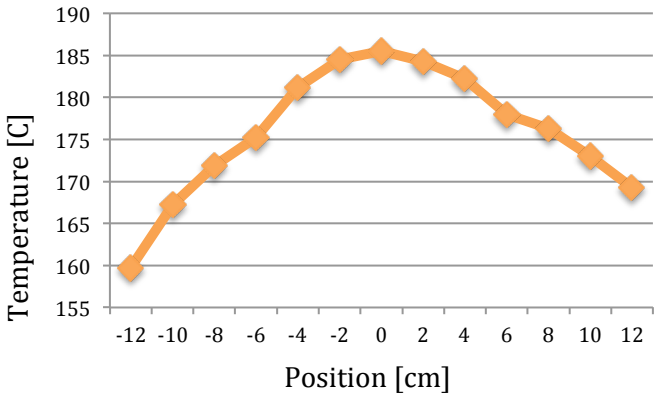


Figure 7. A temperature profile with, temperature against position in centimetre. Zero is at the warmest spot of the furnace.

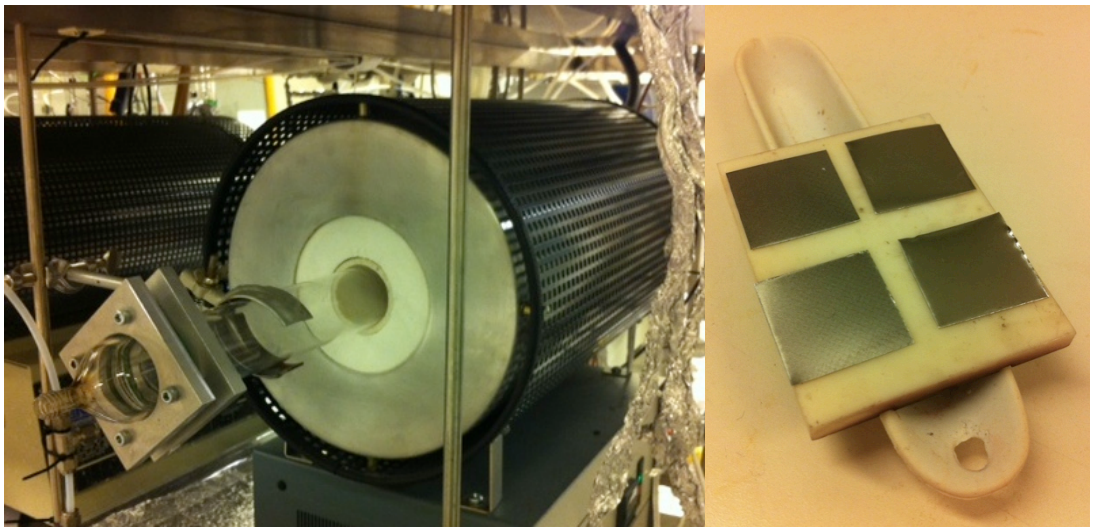


Figure 8. The samples were placed horizontal in a tubular furnace to keep the phosphoric acid evenly distributed at the surface.

The samples were placed horizontal in tubular furnaces, see figure 8, and exposed during one or three weeks. There were 4-8 samples in the furnace at the same time, placed horizontal to keep the phosphoric acid to stay uniform on the entire area. The type of gas, exposure time, temperature and humidity were alternated to arrange different experimental setups. In figure 9 the test parameters are listed.

Cathode	Anode	Temperature	Humidity	Time
Air	Ar – 5 % H_2	25 °C	1-3 % water	1 week
		180 °C	25 % water	3 weeks

Figure 9. The test parameters that were varied into different experimental setups.

The experiments with air as inlet gas flow are a simulation of the cathodic side in a HTPEM fuel cell. The experiments with H_2/Ar gas in the inlet are a simulation of the anodic side in a HTPEM fuel cell, the gas flow contains 5 % hydrogen and 95 % argon gas. The gas flow was regulated to be in total 1000 ml/min for the cathode exposures and 200 ml/min for the anode. It was assumed that the access of oxygen was independent of the gas flow so the flow could be different for the both exposures. The temperature was set to 180 °C during all exposures, except one exposure that was performed in room temperature to see how oxidative the environment is in a non active fuel cell. The humidity was lowered during one exposure to see how the humidity was influencing the corrosion behaviour, from 25 % to 1 % absolute humidity. To see the effect of time and get an indication of corrosion rate the exposure time was extended with two weeks for one exposure, from one week (168 hours) to three weeks (504 hours). In figure 10 the parameters from figure 9 are combined into different exposure environments.

Air	Air	Air	Air	Ar – 5 % H_2
3 % water	1 % water	25 % water	25 % water	25 % water
25 °C	180 °C	180 °C	180 °C	180 °C
1 week	1 week	1 week	3 weeks	1 week

Figure 10. The test parameters combined into different exposure environments.

3.2.4 Cleaning after exposure

To be able to compare mass change and appearance of the samples they were cleaned from phosphoric acid and metal degradation residues. The cleaning was performed in 10 ml distilled water for 10 minutes in an ultra sonification bath at 40 °C. Then the samples were placed in the ultra sonification bath at 30 °C for 10 minutes in acetone and 10 minutes in ethanol. The distilled water was collected and was later on used for analysis, see section 3.8.

3.3 Contact angle

The machine Dat1100 from Fibro system was used to investigate surface interaction of unexposed 316L and MP coated 316L to understand more about the difficulties with adding phosphoric acid on to the steels. The contact angle was measured with 5 M phosphoric acid and with a drop size of 4 µm.

3.4 Photography and Microscopy

After cleaning, the exposed samples were photographed with Canon EOS-1Ds Mark III and investigated in Zeiss microscope at magnifications of 5, 20 and 50 times.

3.5 XRD

A Siemens D5000 powder diffractometer was used to determine the corrosion products. The samples were exposed to a CuK_{α} radiation (λ=1.5418) at an incident angle of 2°. A low angle was used to achieve information about the corrosion product and the substrate. The moving detector collected data in the range of $1° < 2\theta < 70°$ with a step size of 0.05°. The result was then compared to a database with known compounds. One sample from an anodic environment and one sample from a cathodic environment (180 °C, 25 % humidity and 168 hours) were investigated to compare their corrosion products.

3.6 SEM

To investigate the corrosion products SEM with EDX was used. One sample from an anodic environment and one sample from a cathodic environment (180 °C, 25 % humidity and 168 hours) were gold coated and embedded into epoxy. The two samples were grinded and polished to achieve a cross sectional surface.

3.7 Resistance measurement

The resistance of an exposed sample was measured with different methods. A large part of the time spent on laborative work was focused on investigation and development of a better method for measuring the resistance.

The first equipment used for measuring the resistance in the samples, see figure 11A, was constructed with electrodes that measure the resistance over time. The resistance was measured with an applied pressure of 140 N/cm^2 during 1000 s. Two different electrode sizes were examined, 15x15 mm^2 and 5x5 mm^2. The small electrode made it possible to do a few comparable measurements at the same sample and also measure a more specific area. The resistance varied over time but tended to stabilize after 500 s. Therefore an average of the values between 500-1000 s was used. This method for measuring the resistance was not satisfying; the values were fluctuating widely due to other reasons than amount of corrosion.

To get more accurate result, another method was tested. The samples were painted with fast drying silver paint. Three circular areas were painted at each sample, two replicates for each sample. A multimeter was used to get the resistance value for the specific area. See picture B figure 11. The multimeter did not settle and therefore no values could be achieved.

A third method was examined. By using aluminium foil gaskets, with a diameter of 5mm, gold was sputtered on the samples for 10 minutes at 40 mA. A multimeter was used to measure the resistance. The backside of the sample was grinded to achieve a better contact with the multimeter. See picture C in figure 11. Two 316L samples from each type of exposure setup was examined, except for the exposure in room temperature where only one sample was tested and the three weeks exposure was not tested at all. Two MP samples were also tested from the cathodic exposure in 180 °C at 25 % humidity for 168 hours.

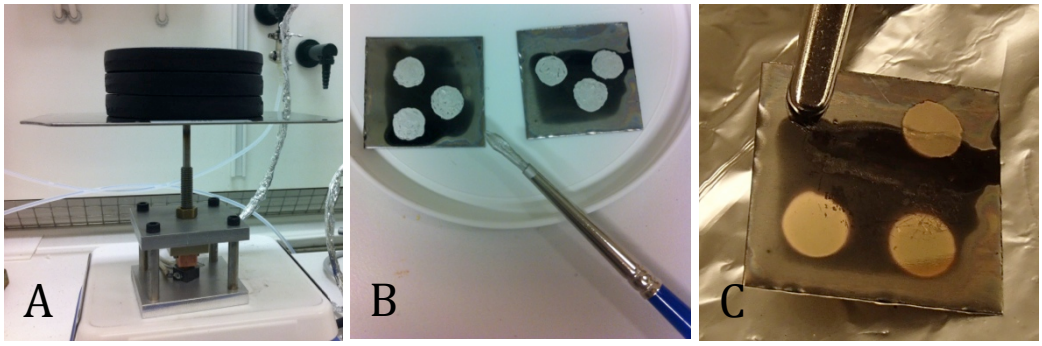


Figure 11. The figure shows three different resistance measurements methods.

3.8 ICP-AES

The wash water from the exposed samples (see section 3.2.4) was used for ICP-AES analysis. 3 ml from the wash water was diluted with nitric acid to a total volume of 50 ml. A calibration curve for chromium, iron and nickel, was created from standard solutions. For ICP-AES a Termo Scientific ICAP 6000 Series was used. Washing water from five different samples was collected. Water from two samples from an exposure in a cathodic environment at 180 °C in 25 % humidity for 168 hours, one 316L and one Max Phase coated 316L. Water from two samples from an exposure in an anodic environment at 180 °C in 25 % humidity for 168 hours, one 316L and one Max Phase coated 316L. Last, water from one Inconel 625 sample, the anodic exposure only.

4. Results

4.1 Contact angle

The contact angle is interesting for the insight in how phosphoric acid is behaving on the surface of stainless steel. During spraying, 316L achieved a smooth layer of phosphoric acid and MP coated 316L got the surface covered with small drops of phosphoric acid. The contact angle for 5 M phosphoric acid at 316L and 316L coated with MP, at room temperature, can be seen in figure 12 and 13.

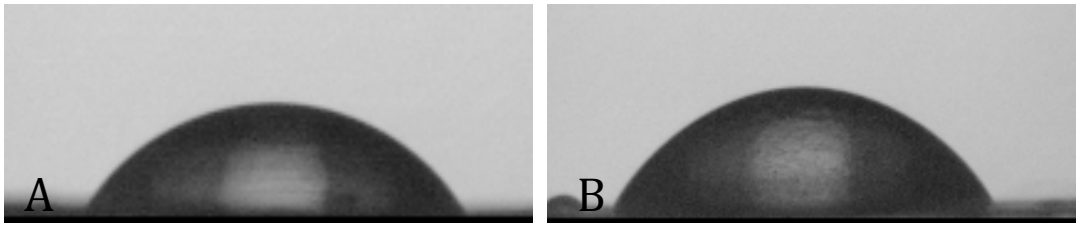


Figure 12. A) The contact angle for 5 M phosphoric acid at unexposed stainless steel 316L. B) The contact angle for 5 M phosphoric acid at MP coated stainless steel 316L.

The pictures in figure 12 illustrates that MP have a slightly less hydrophilic surface than 316L, which explains why it is a little more problematical to cover MP with phosphoric acid during spraying. The less hydrophilic behaviour can be a combination of the surface energy and the roughness of the netlike surface structure of MP [37]. Due to this matter the samples are placed horizontal in the furnace to keep the phosphoric acid stay even on the surface during the exposure.

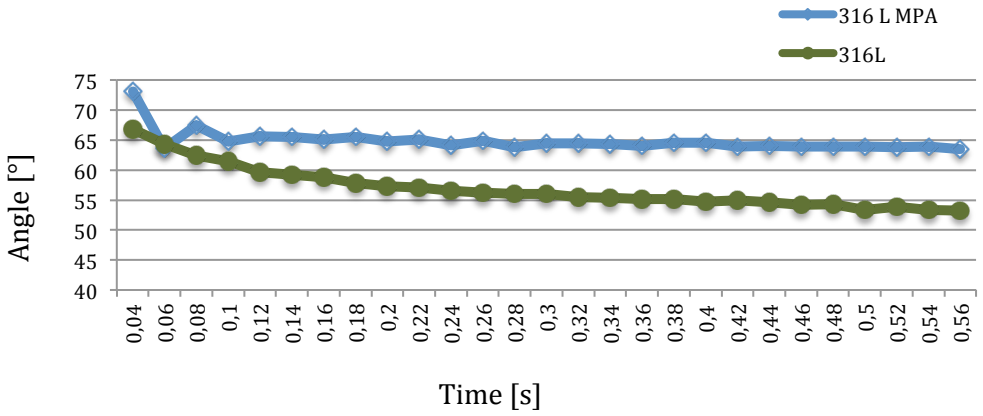


Figure 13. The contact angle for 5 M phosphoric acid at stainless steel 316L and at MP coated stainless steel 316L. Observe that the y-axis starts at 40°.

4.2 Photography and Microscopy

Photographs were taken after cleaning the exposed samples. The images contain 4 samples each, the upper two are 316L and the lower two are MP coated 316L. The samples chosen are representative for the exposure.

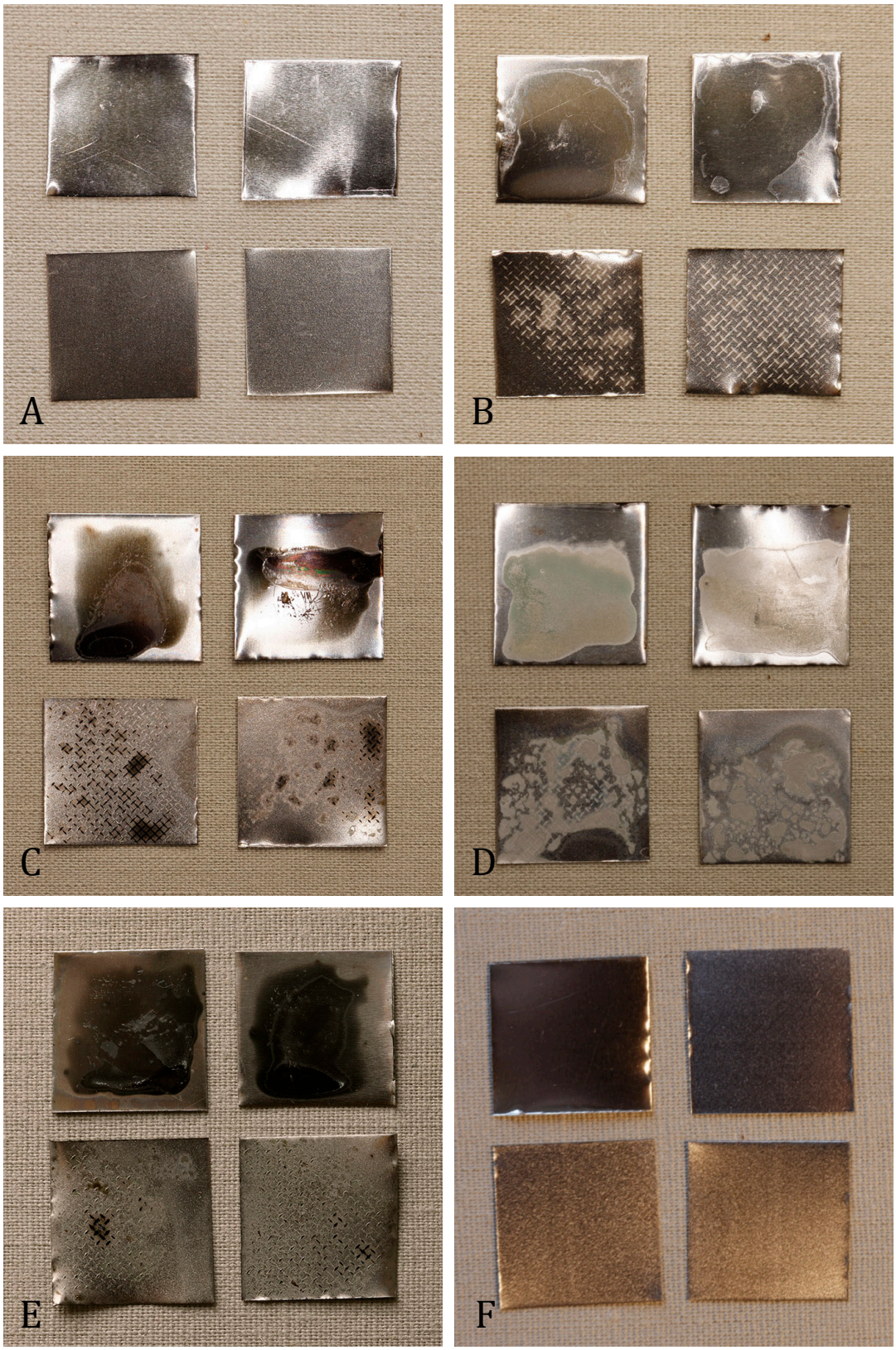


Figure 14. Photographs taken after washing the samples after exposure. In every picture the two upper samples are 316L and the two lower are MP coated 316L. A) Cathodic environment at 25 °C, 3 % humidity for 168 hours. B) Cathodic environment at 180 °C, 1 % humidity for 168 hours. C) Cathodic environment at 180 °C, 25 % humidity for 168 hours. D) Anodic environment at 180 °C, 25 % humidity for 168 hours. E) Cathodic environment at 180 °C, 25 % humidity for 504 hours. F) Reference study, samples without phosphoric acid exposed to a cathodic environment at 180 °C, 25 % humidity for 168 hours,

Microscopic images were taken at 50x magnification on unexposed samples to use as comparison to exposed samples. Figure 15A is an image of a 316L sample and 15B is an image of a MP coated 316L sample.

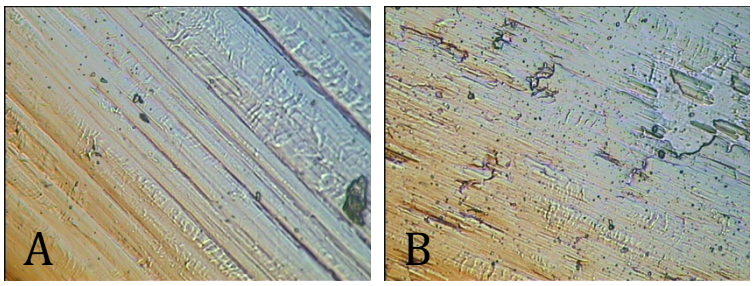


Figure 15. Microscopic images of unexposed samples at a magnitude of 50 times. A) 316L sample B) MP coated 316L sample.

When comparing the microscopic pictures of the 316L samples from a hydrogen/argon environment with microscopic pictures of a sample from an exposure in air, the samples look different, see figure 16 and compare A-C with D-F. The samples from the exposure in air have a dark surface with cracks at some parts. The cracks can be seen in the picture of 50x magnification, figure 16C. The samples from the hydrogen environment have an unsmooth surface that are covered with crystals and on top probably a thin layer of phosphoric acid. Figure E and F show the point where the unsmooth surface meets the unoxidized stainless steel.

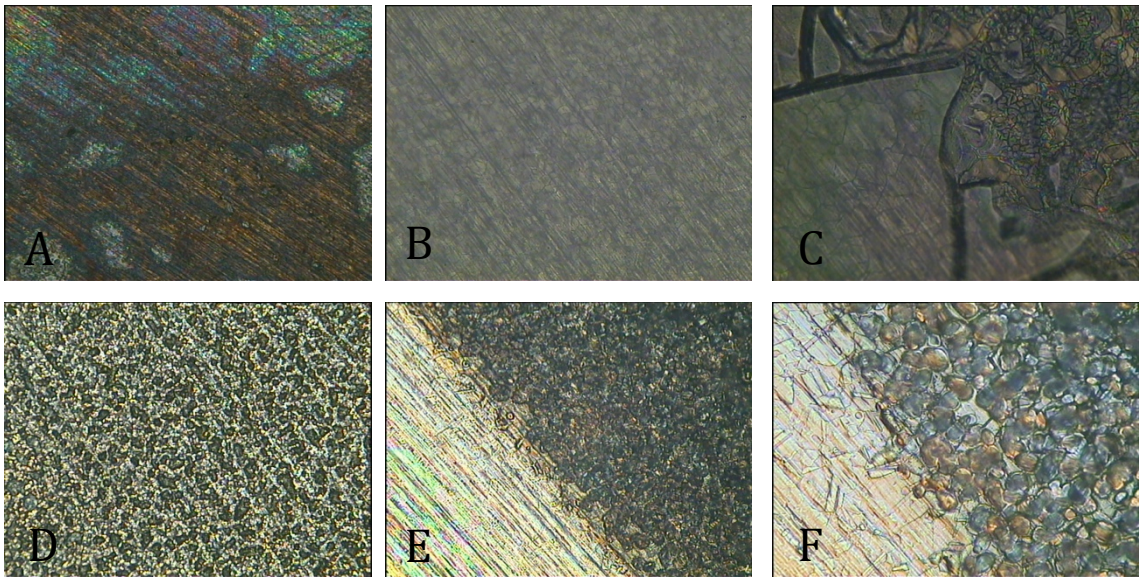


Figure 16. A-C) Microscopic images of a 316L sample exposed to a cathodic exposure in 180 °C and 25 % humidity for 168 hours. The images are taken at a magnitude of 5, 20 and 50 times (left to right) D-F) A 316L sample exposed to an anodic exposure in 180 °C, 25 % humidity for 168 hours. The images are taken at a magnitude of 5, 20 and 50 times (left to right).

Microscopic images of 316L samples coated with MP can be seen in figure 17. The microscopic picture of 5x magnification illustrates the oxidation located in a net-like structure. This structure is more obvious for the cathodic exposures than the anodic exposures.

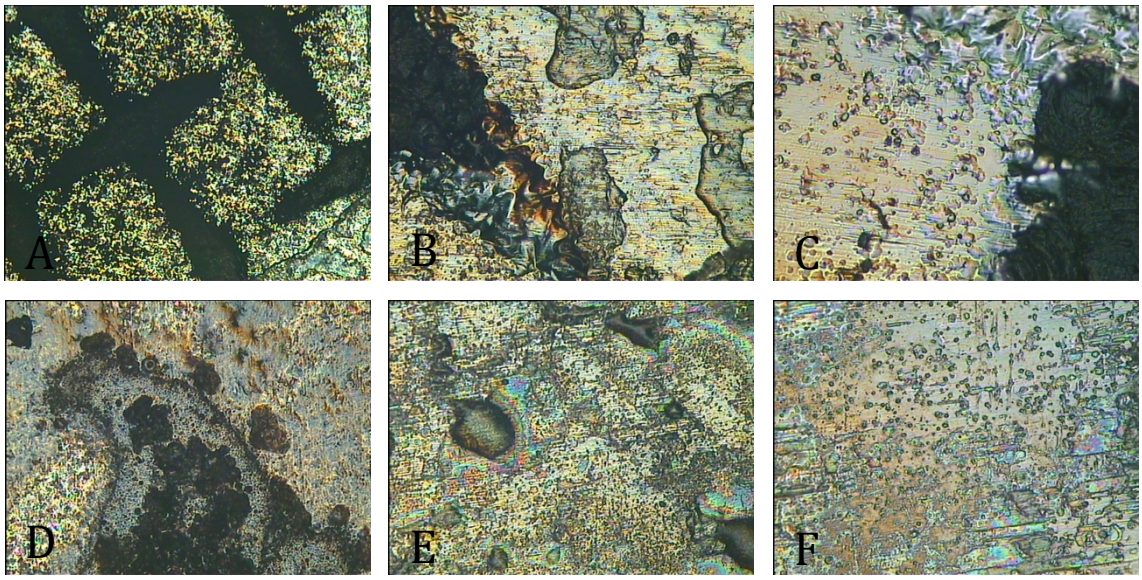


Figure 17. A-C) Microscopic images of a MP coated 316L sample exposed to a cathodic exposure in 180 °C and 25 % humidity for 168 hours. The images are taken at a magnitude of 5, 20 and 50 times (left to right) D-F) A MP coated 316L sample exposed to an anodic exposure in 180 °C, 25 % humidity for 168 hours. The images are taken at a magnification of 5, 20 and 50 times (left to right).

4.3 XRD to examine the corrosion products

XRD was used to achieve crystallographic information about the corrosion product at the samples. Achieved from the XRD was a spectra for a sample exposed to a cathodic environment at 180 °C in 25 % humidity for 168 hours, see figure 18. The spectrum has two large peaks, one at ~43.5 ° and one at ~51 °, that match the peaks for austenite stainless steel 316L known from a reference sample. When no other peaks can be found, and the spectra consisted of a bump characteristic for amorphous materials, the conclusion is that the corrosion product for the cathodic exposed 316L was amorphous [38].

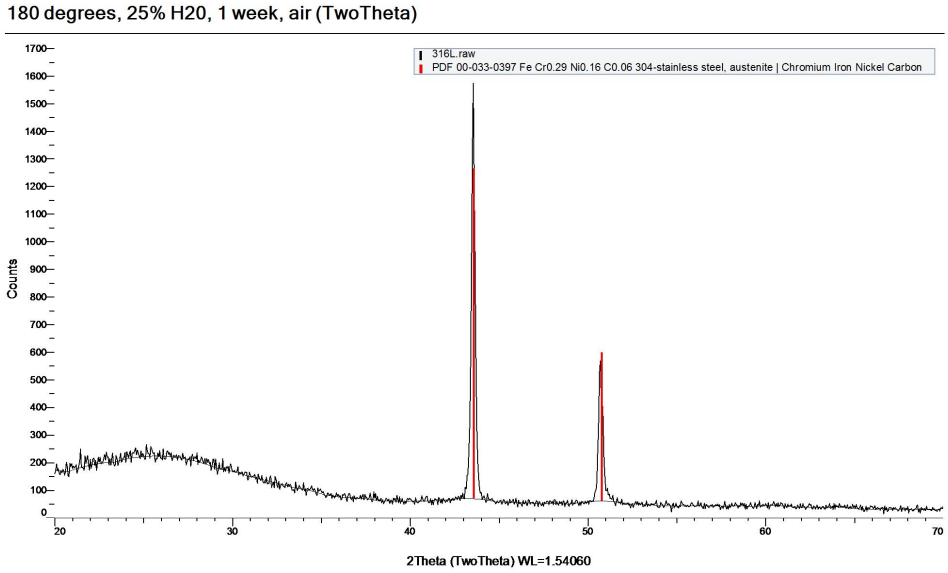


Figure 18. The XRD spectra for the cathodic exposure in 180 °C and 25 % humidity for 168 hours.

The spectra in figure 19, is for a sample exposed to an anodic environment at 180 °C in 25 % humidity for 168 hours. The spectra shows partly the same peaks as the previous spectra, ~43.5 ° and ~51 °, but it also consist of many other peaks. This lead to the conclusion that the samples exposed to anodic environment have crystalline corrosion products, but maybe also additional amorphous products. The best match found in the database was with iron hydrogenophosphate, $FeH_2P_2O_7$. Two samples for each environment were tested to confirm the results.

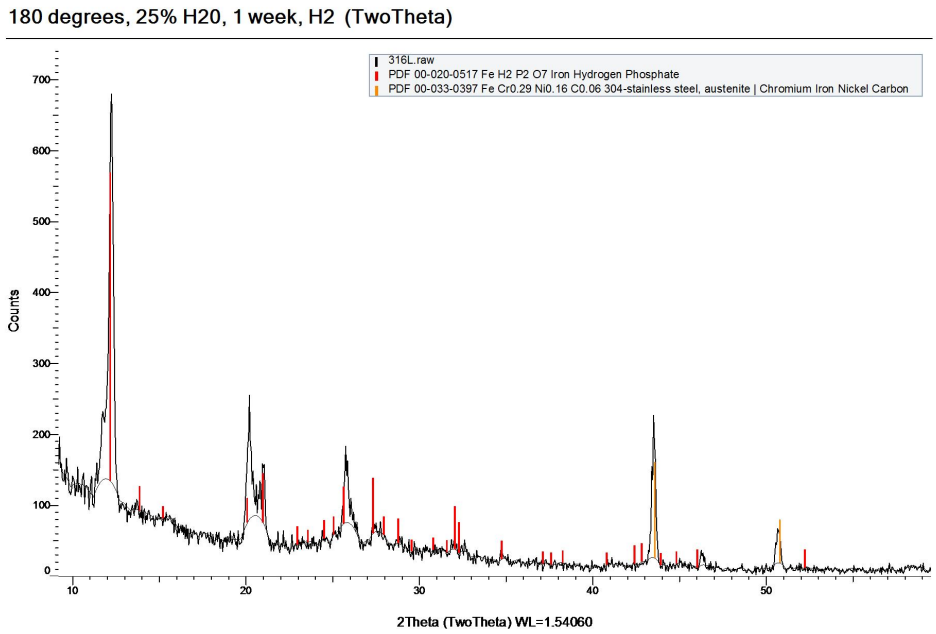


Figure 19. The XRD spectra for the anodic exposure in 180 °C and 25 % humidity for 168 hours.

4.4 SEM-EDX to examine the corrosion products

The SEM images of the cross sections look similar for the anodic and the cathodic exposure for 168 hours in 180 °C and 25 % humidity, see figure 20, but there are one main difference between the images. The corrosion scale is thicker for the cathodic exposure than the anodic exposure, and it has a more layering structure.

The composition of the corrosion products are obtained from an average of two/three different spectra at the cross-section area, see the orange rectangles at the SEM pictures. The values from the different spectra did not differ much. The compositions are in percentage and are rounded to the nearest integer; see the two diagram pies in figure 20. EDX contributes with an approximate chemical composition and the results can be used to confirm the same type of corrosion product that XRD suggested for the anode exposure, $FeH_2P_2O_7$. The composition of the sample from the anodic exposure environment has the same approximate chemical composition as the sample from the cathodic exposure environment.

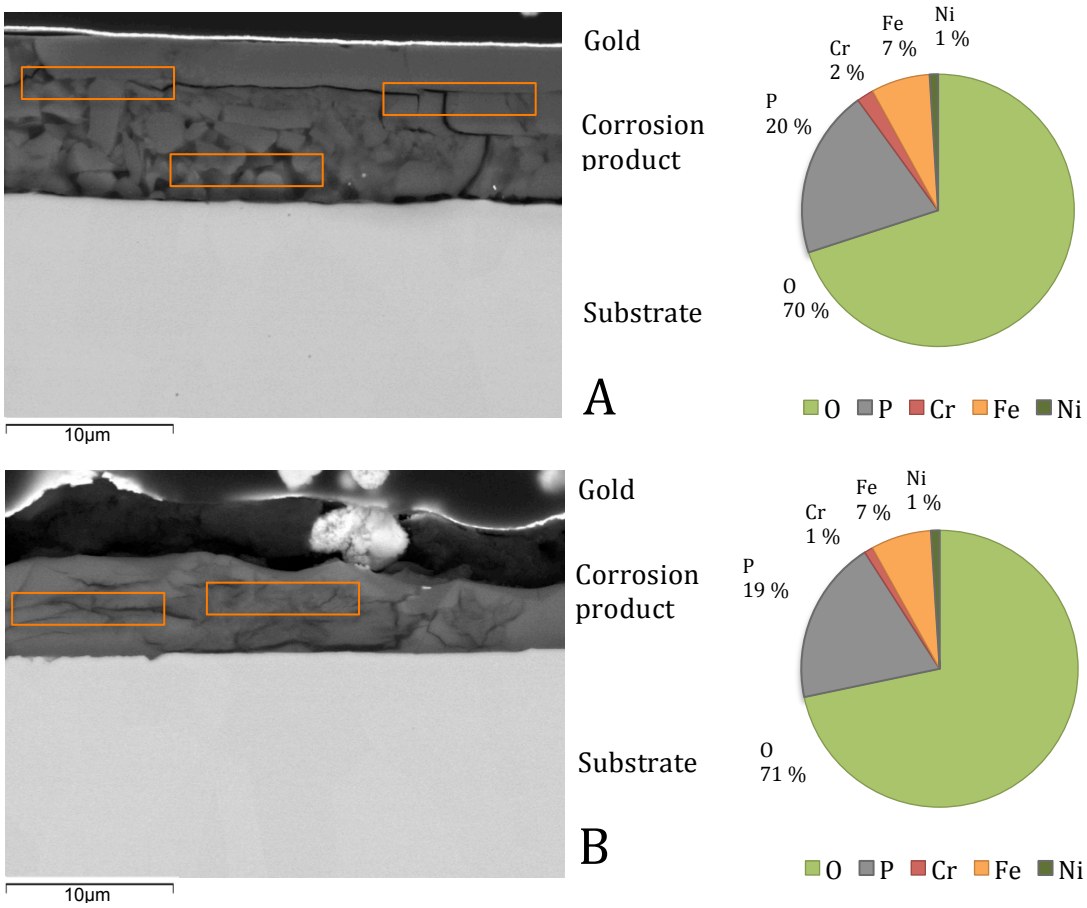


Figure 20. SEM images of cross-sections and the average amount of each component in orange rectangular areas illustrated in a pie diagram. A) A 316L sample exposed to a cathodic exposure in 180 °C in 25 % humidity for 168 hours. B) A 316L sample exposed to an anodic exposure in 180 °C in 25 % humidity for 168 hours.

4.5 Mass change for quantification of corrosion

The mass change can be used for quantification of corrosion. The mass change is a value of the weight after washing with the weight of the samples before exposure subtracted. The mass change then corresponds to the formed oxide products but also taking into account the metal ions that may have been dissolved from the metal during oxidation, the uptake subtracting the dissolution. The mass changes in average of all 316L samples are presented in figure 21, and for MP coated 316L samples from two exposures, the cathodic and anodic exposures in 180 °C and 25 % humidity for 168 hours.

The 316L samples exposed to room temperature, 3 % humidity and air, have an average mass change that is close to zero, 0.0015 mg/cm^2. The 316L samples exposed in cathodic environment at 180 °C and 1 % humidity for 168 hours, have a small negative average mass change of -0.076 mg/cm^2. The mass change for the cathodic exposure of 316L, in 180 °C and 25 % humidity for 168 hours, is high compared to the other values, with an average mass change of 0.52 mg/cm^2. The anodic exposure of 316L, in 180 °C and 25 % humidity for 168 hours, has lower values than the cathodic exposure in 180 °C and 25 % humidity, 0.073 mg/cm^2. The exposure in a cathodic environment at 180 °C and 25 % humidity for three weeks has the highest value, 0.62 mg/cm^2. The MP coated 316L samples have a negative average mass change

of -0.093 mg/cm^2 for the cathodic exposure and a low average mass change of 0.0068 mg/cm^2 for the anodic exposure. The mass change for the other MP coated 316L samples are not included in the graph in figure 21.

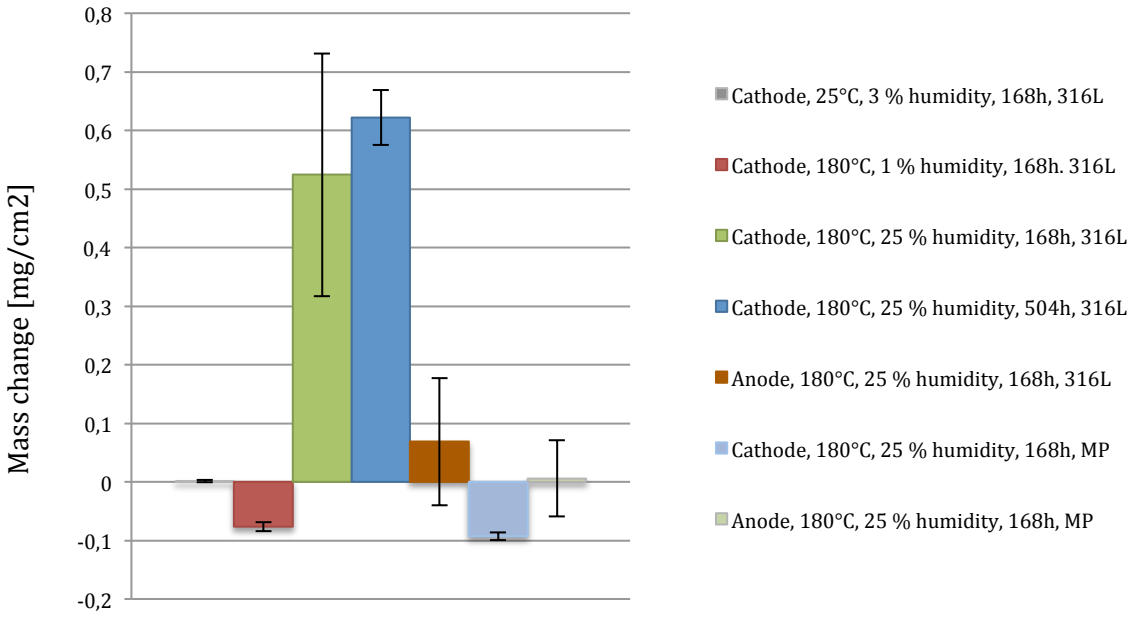


Figure 21. The mass change in mg/cm^2 for 316L exposed to different environments and MP coated 316L. The standard deviation is marked with an error bar. The largest mass change is for the samples exposed to a cathodic environment during three weeks.

4.6 Resistance for quantification of corrosion

Electrical resistance measurements could be used as a method to quantify the amount of corrosion at different samples. The resistance is expected to be proportional to the thickness of the oxide. These resistance measurements are only used as a comparative study. None of the methods for measuring the resistance gave reliable results but gave some indication of which environments that caused more severe corrosion.

The values from measuring the resistance with the experimental setup for current project, see figure 11A, were not satisfying. The resistance measured at a specific spot of an exposed sample could change between different measurements. The fluctuation could be due to the pressure, how hard the screw was screwed or the small difference in angle of the electrode when it was pressed down against the sample. The results were consequently not used for comparing oxidation.

Measuring the resistance with a multimeter at the silver painted circular areas at the exposed samples was impossible. The values shifted between 3 Ω and 10 MΩ, and did not stabilize.

The third method used, where gold was sputtered using a defined sputter shadow mask into uniform electrodes on the samples, see figure 11C. Measuring resistance gave more reproducible results than the two previously tested methods, but was still not satisfying. A multimeter was used to measure the resistance at gold sputtered circular areas at the samples, see table 2. The resistance was low and similar for all samples and environments except for the both samples from the cathodic exposure in 180 °C and 25 % humidity for 168 hours. These

samples have higher values in general, and two values that are much higher. This can indicate that the oxidation during exposure was higher for those samples.

Table 2. Table with the resistance values from the third resistance method with the gold sputtered circles on the samples.

Sample [Ω]	Cathode: 25 °C, 3 % H_2O, 168 h, 316L	Cathode: 180 °C, 1 % H_2O, 168 h, 316L	Cathode: 180 °C, 25 % H_2O, 168 h, 316L	Anode: 180 °C, 25 % H_2O, 168 h, 316L	Cathode: 180 °C, 25 % H_2O, 168 h, MP
Sample 1	0.4	0.2	1.1	0.6	0.9
Sample 1	0.6	0.2	1.8	1.3	0.3
Sample 1	0.6	0.4	85000	0.7	0.2
Sample 2	-	0.9	200	0.2	0.3
Sample 2	-	0.1	0.7	0.4	0.1
Sample 2	-	0.1	19000	0.8	0.3
Average	**0.53**	**0.32**	**17367.27**	**0.67**	**0.35**

4.7 ICP-AES for quantification of corrosion

The emission spectrometry experiments contribute with an indication of the composition of ions in the washing liquid. The ions in the washing liquid are a measure of what water-soluble ions that have been washed away from the samples after exposure. The amount of ions then indicates the grade of degradation during exposure, due to dissolution of metal ions. It is important to know that these experiments were performed with only one sample from each exposure. The ions present with highest concentration where nickel, chromium and iron, and these ions were used for quantification of corrosion, see figure 22.

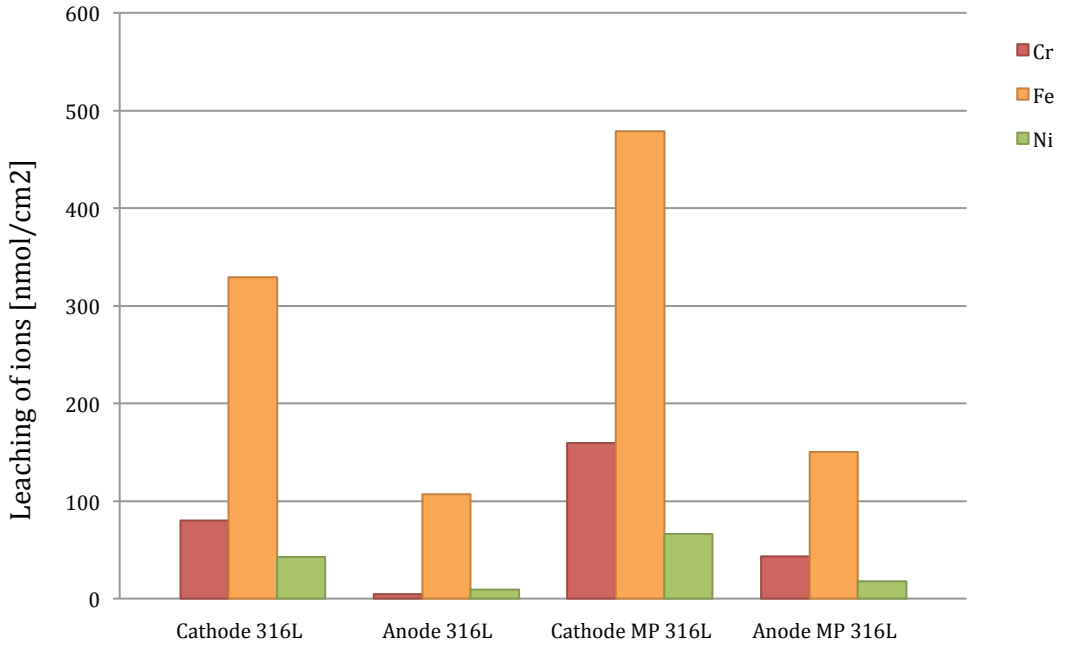


Figure 22. The amount of leached ions in the washing liquid, nmol/cm^2. Values based on only one sample.

When comparing the analysis of the washing liquid from the anodic and the cathodic exposure of 316L, in 180 °C and 25 % humidity for 168 hours, there was no difference in the present ions but the concentration of ions differed. The cathodic exposure has a larger amount of iron, nickel and chromium, see figure 22. If comparing the result for the 316L samples with the MP coated 316L samples, there seems to be more leaching of ions for the MP coated samples.

4.8 Inconel 625

The comparison between Inconel 625 and stainless steel 316L are done with photographs, mass change and ICP-AES. When observing figure 23A, with one 316L sample and one Inconel 625 sample, both exposed to a cathodic exposure environment for one week, 168 °C and 25 % humidity, a large difference is noticed. Inconel 625 does not seem to consist of an oxide, but there might have occurred some dissolution of the metal during exposure. The same suggestion is for 23B were the Inconel 625 and stainless steel 316L have been exposed to an anodic exposure environment for one week, 168 °C and 25 % humidity.

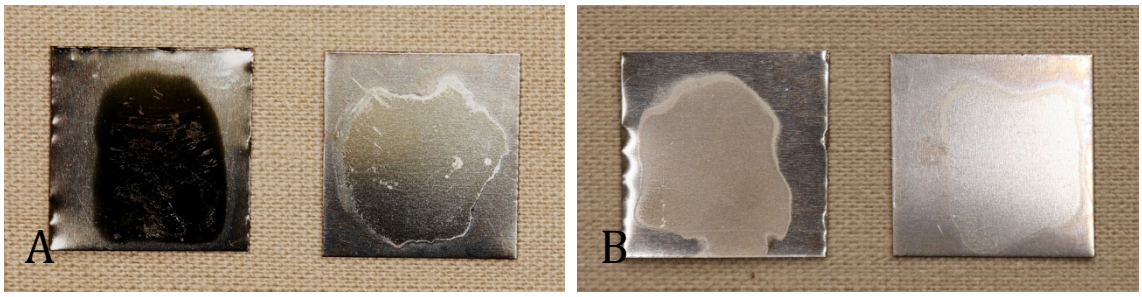


Figure 23. Photographs of an Inconel 625 sample next to a 316L sample. Inconel 625 is to the right in the photographs. A) A comparison between a 316L sample and an Inconel 625 sample exposed to a cathodic environment at 180 °C in 25 % humidity for 168 hours. B) A comparison between a 316L sample and an Inconel 625 sample exposed to an anodic environment at 180 °C in 25 % humidity for 168 hours.

Figure 24 shows the mass gain for Inconel 625. The mass gain is negative for all samples, the average is -0.0016 mg/cm^2 for the exposure in humidified air and 0.0015 mg/cm^2 for the exposure in humidified hydrogen. The mass gain for Inconel 625 is lower than for 316L exposed to the same environment.

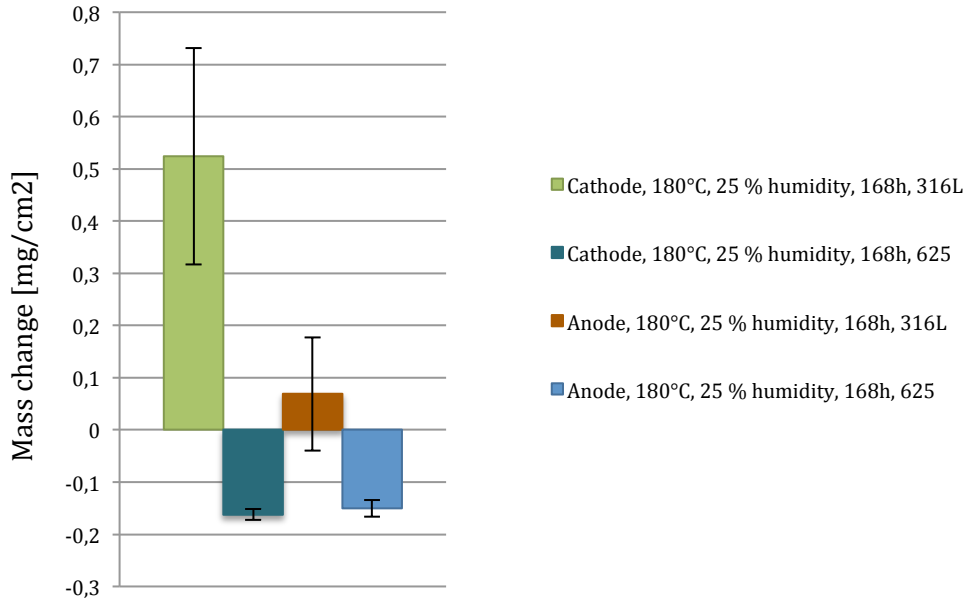


Figure 24. The mass gain for Inconel 625 compared to 316L in both the cathodic exposure environment at 180 °C in 25 % humidity for 168 hours and the anodic environment at 180 °C in 25 % humidity for 168 hours.

In figure 25 the amount of leached ions is compared between 316L and Inconel 625. Both samples are from an anodic exposure environment with 25 % humidity and 180 °C. When observing figure 25 it can be seen that Inconel 625 has a higher total amount of leached ions during washing after exposure than 316L. The ion composition of unexposed 316L and Inconel 625 is different and need to be taken into account when comparing the amount of leached ions. If comparing the composition of unexposed 316L with unexposed Inconel 625, see table 1, the amount of iron is 67 % for 316L compared to 5 % for Inconel 625, which could explain why the iron leaching is higher for 316L even if the loss of metal ions and the degradation may be larger for Inconel 625.

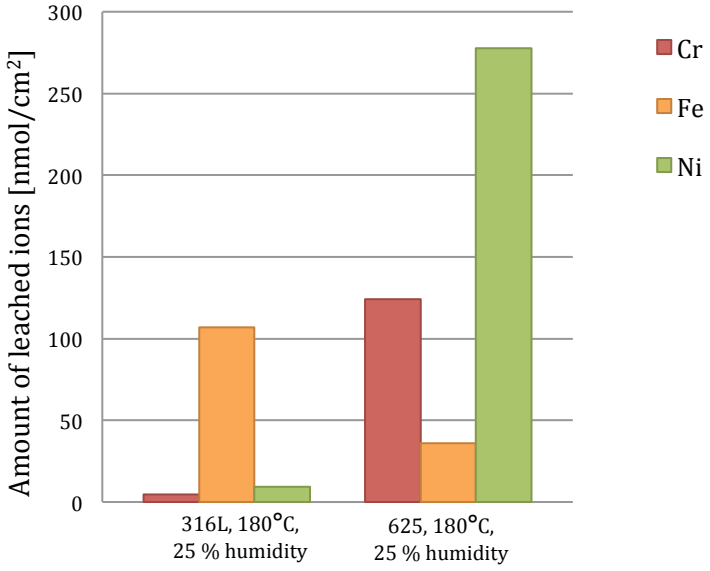


Figure 25. The amount of leached ions in the washing liquid in nmol/cm^2. The sample from the anodic environment for 316L, in 180 °C and 25 % humidity for 168 hours, compared to an Inconel 625 from the same environment. Based on only one sample.

5. Discussion

The discussion will be divided into four parts, the first two parts are regarding the corrosion products and quantification of the corrosion. The third part discusses how alternating environmental parameters, such as temperature, humidity or atmosphere during furnace exposure affects corrosion, and a discussion about which environmental parameter that is most corrosive. The last part discusses Inconel 625.

5.1 Corrosion product

The corrosion products have been investigated with photography, microscopy, XRD and SEM. The corrosion product on the samples looks different for samples exposed to a cathodic environment compared to samples exposed to an anodic environment. The cathodic corrosion product is black (see figure 14, A-C and E), and the anodic corrosion product is light green (see figure 14D). This can indicate different corrosion products.

When using XRD to examine the corrosion product at the sample exposed to cathodic environment for 168 hours in 25 % humidity and 180 °C, the only achieved peaks corresponded to the metal substrate, see figure 18. The lack of peaks for the corrosion product lead to a conclusion that the corrosion product formed is amorphous. The XRD result for the sample exposed to the anodic environment for 168 hours in 180 °C and 25 % humidity had peaks corresponding to both the metal substrate and the corrosion product, see figure 19. The corrosion product was proposed to be $FeH_2P_2O_7$. SEM with EDX results suggested a chemical composition that was in agreement with the suggested product from the XRD for the anode exposure, $FeH_2P_2O_7$. If comparing the pie diagrams in figure 20, for the anodic and cathodic exposure, their composition are almost the same, therefore a suggestion is that the corrosion product for the cathodic exposure in 180 °C and 25 % humidity is $FeH_yP_2O_7$. The hydrogen amount cannot be told without more information due to the low energy for hydrogen atoms. The amount of hydrogen can affect the valence of the metal ions and thereby maybe change the oxide growth. A change in oxide growth could be a reason for an amorphous corrosion product for the cathode exposure compared to a crystalline product for the anode exposure.

The SEM pictures of the cross sections look similar for the anodic and the cathodic exposure for 168 hours in 180 °C and 25 % humidity, see figure 20. The corrosion product is thicker for the cathodic exposure than the anodic exposure. A thicker corrosion product is an indication of a more corrosive environment, but it is not definite that the corrosion product has a homogenous thickness for the complete surface, and during SEM only a small fraction of the whole area was investigated.

The images from the light microscope shows a dark smooth surface for the samples from the cathodic environment, but a less smooth surface for the light green samples from the anode exposure. The anodic samples have a hilly surface, and are probably consisting of a crystalline oxide product with a thin layer of phosphoric acid covering it.

S. Molin et al. have investigated the oxide products that are formed on stainless steel 316L in 400 °C and 800 °C [39]. Their samples were oxidized in air and in humidified hydrogen for 300 hours. The samples were not sprayed with phosphoric acid and the experiments were performed at high temperature, so the relevance when comparing to results in this project is to consider. The oxide product formed at samples during S. Molin et al. experiments exposed to airflow is

dark grey/black and the samples exposed to the hydrogen atmosphere has a green oxide scale, which corresponds to the result in current project. In the article they claim that the difference in colour of the oxide product can be due to the difference in oxide scale growth. Their suggestion may then be the reason for the colour difference of the corrosion product in this project. The difference in oxide growth may then influence the oxide product in a way that one has time to arrange its atoms in a crystalline order and the other becomes amorphous. This may then also affect the colour of the oxide product, how the light is reflected. The difference in colour can also be depending on the oxidation state for the iron in the corrosion products. Fe^{2+} is known to affect its compounds with a pale green colour and this could be the reason for the colour of the corrosion product on the sample exposed to hydrogen atmosphere. The oxidation state for iron may then be Fe^{3+} for the corrosion product on the samples exposed to air, which led to the dark grey colour.

5.2 Quantification of corrosion

The quantification of the corrosion at the samples was done by comparing photographs, values of mass change, resistance measurements and ICP-AES results. Mass change can give an indication about the amount of oxidation that occurred during exposure. The measured mass changes in the current project were small, thus it was difficult to distinguish in a realistic way due to low values. The weight difference is small due to small samples and relatively mild oxidation of the stainless steel. It is hard to know if the difference in mass change is due to the formation of a corrosion product, loss of stainless steel due to degradation or a combination of both. A negative value may correspond to a loss of metal ions due to degradation and no formation of an oxide layer.

The mass change indicates that the most oxidative exposure environment is the cathodic environment with 25 % humidity and 180 °C, see figure 21. The one-week exposure in this environment has an average mass change of 0.52 mg/cm^2 and the three-week exposure has a mass change of 0.62 mg/cm^2. The mass change indicates that the cathodic exposure environment is more corrosive than the anodic exposure environment. The average mass change for 316L samples from the cathodic exposure in 180 °C and 25 % humidity for 168 hours is 0.52 mg/cm^2, compared to the anodic exposure with an average mass change of 0.073 mg/cm^2.

The third resistance measurements method, where the samples had been sputtered with gold electrodes, gave results that suggests that the cathodic environment at 180 °C and 25 % humidity is the most corrosive environment, but the method cannot give a reliable result but still a strong indication. The resistance was low and similar for all samples except the samples from this cathodic exposure in 180 °C and 25 % humidity for 168 hours, these samples have higher values in general, and two values that are much higher, see table 3. The reason for the low values could be that they are below the noise level and cannot be detected properly compared to the cathodic samples in 180 °C and 25 % humidity, and there maybe a short circuit in the material. The corrosion observed seem to be localized and this method may work better if the gold electrodes had a smaller area.

ICP-AES was performed on washing liquid from 316L samples exposed to a cathodic environment at 180 °C, 25 % humidity for a week and 316L samples exposed to an anodic environment at 180 °C, 25 % humidity for a week. When comparing the washing liquid from the anodic and the cathodic exposure there were no difference in components but the amount of ions differed. The cathodic exposure has a larger leaching of iron, nickel and chromium, see

figure 22. The leaching of ions during washing of the samples after exposure is related to the oxidation of samples during exposure, and more leaching of ions out in the washing water can be an assumption that more degradation has occurred to the sample.

5.3 Parameters

There are many parameters that may affect the oxidation of 316L samples during furnace experiments; temperature, humidity, exposure time, gas composition and coatings.

5.3.1 Temperature

By looking at the samples 316L and 316L coated with MP, exposed to a cathodic environment at room temperature for 168 hours, indicates that nothing occurred during the exposure, see figure 14A. The weight gain of the samples is negligible with an average mass gain of 0.0015 mg/cm^2 for a 316L sample. The microscopic pictures, figure 26, looks almost the same as the unexposed microscopic pictures, figure 15A and B. This strengthens the suggestion that very little has happened, due to effective passivation, during room temperature exposure for samples of stainless steel 316L during 3 % humidity and a cathodic environment for 168 hours.

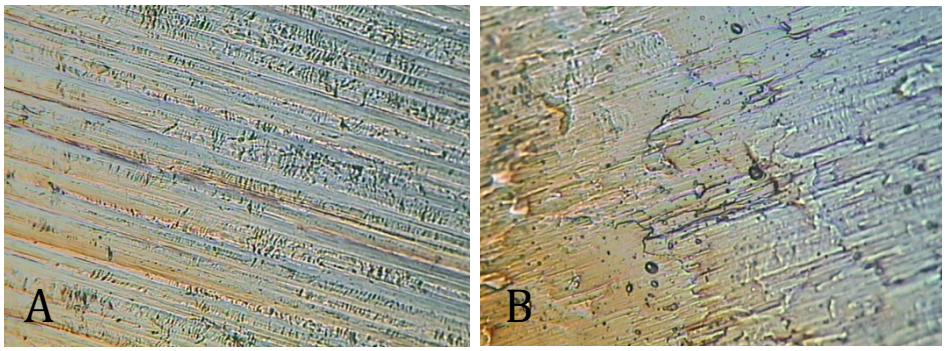


Figure 26. Microscopic pictures of samples that have been cleaned after exposure in a cathodic environment, with 25 % humidity for 168 hours, at room temperature. A) 316L at a magnification of 20 times. B) 316L coated with MP at a magnitude of 50 times.

5.3.2 Humidity

Photographs and mass change both indicate that lower humidity results in lower oxidation, which can be noticed when comparing figure 14B and 14C. Figure 14B corresponds to a humidity of 1 % and figure 14C to a humidity of 25 % during a cathodic environment exposure for 168 hours and 180 °C. At 14B no oxide product can be seen but maybe a loss of metal ions due to degradation, and the negative mass gain of -0.076 mg/cm^2 for 316L also indicates a loss of metal ions during exposure. The mass change before and after exposure is much lower for the samples exposed to a lower humidity, see figure 21.

5.3.3 Atmosphere

The results from mass change, microscopy and ICP-AES all indicates the same thing: that the environment during anodic exposure is less corrosive than the environment during cathodic exposure. Figure 14C shows samples exposed to a cathodic environment at 180 °C, in 25 % humidity for 168 hours, and figure 14D shows samples exposed to an anodic environment at 180 °C, in 25 % humidity for 168 hours. The upper samples are the uncoated 316L and the

lower samples are the MP coated 316L. The samples from the cathodic environment seem more oxidized than the samples from the anodic environment, therefore a suggestion is that a cathodic environment is more oxidizing than an anodic environment.

The mass change that can be seen in figure 21 clarifies that the cathodic exposure environment is more corrosive than the anodic exposure environment for samples exposed in 180 °C and 25% humidity for 168 hours. The mass gain is in average 0.52 mg/cm^2 compared to 0.073 mg/cm^2.

When looking at the results from the ICP-AES in figure 22, there can be seen that the samples exposed to a cathodic environment leaches more chromium, iron and nickel ions during washing after exposure than the samples exposed to an anodic environment. The more leaching out of ions in the washing water, the more oxidized are the samples. This strengthens the indication that the cathodic environment is more oxidizing than the anodic environment and a conclusion can be drawn.

5.3.4 Exposure time

When comparing the samples that have been in a cathodic environment at 180 °C, in 25 % humidity for a week, and for three weeks, there is a small difference noticed, see figure 14C and 14E. Comparing the average mass change for the 316L samples, there is a small difference between the one-week exposure and the three-weeks exposure, 0.52 mg/cm^2 compared to 0.62 mg/cm^2, see figure 21. There were some experimental difficulties with the furnace for the three-weeks exposure that may have affected the oxidation and lowered it, there were a lack of water during one day of the exposure due to a too high flow during the weekend. That could be the reason for this low difference in mass change, or it can be that all available phosphoric acid has reacted and the oxidation stopped. If looking at the kinetics for atmospheric corrosion, figure 3, the rate is logarithmic and the oxidation rate will decrease with time. The exposure time does not seem to be the limiting factor in this project but it does affect the samples, more experiments are needed to be able to say anything concrete.

5.3.5 Max Phase Coating

Coating the 316L samples with MP appears to protect the samples slightly from corrosion attack. By studying figure 14, uncoated samples seem to be more oxidized that MP coated. Figure 20 clarifies with the mass change that MP coated 316L has a lower mass change than the uncoated 316L samples. This indicates that the MP coated 316L has a higher resistance to oxidation than the uncoated 316L. The result from the ICP-AES tells that the leaching of ions is higher for MP coated samples than for the uncoated 316L. This indicates that the dissolution is higher during exposure for the coated samples. The MP coated samples may have a more protective oxide layer formed that protects the samples from dissolution. The microscopic image of an MP coated sample, see figure 17A, at a magnitude of 5x, exposed to a cathodic environment for 168 hours in 180 °C and 25 % humidity shows a corrosionpattern as a net-like structure. MP coating was produced by placing the stainless steel on a net and coating it from both sides, this fixture method may then influence the corrosion of the samples by inhomogeneous film thickness.

5.4 Inconel 625

Inconel 625 is more corrosion resistant and expensive than stainless steel 316L, and the difference in performance are investigated to see if it is cost-effective to choose Inconel 625 instead of 316L to be the steel to use in a fuel cell and to be coated with Max Phase coating. Figure 23 indicates that nothing or nearly nothing have happened to the samples of Inconel 625 compared to the oxidation of the 316L samples in a cathodic and anodic environment with 25 % humidity and 180 °C for 168 hours. If comparing the mass change it is clear that only a very thin protective oxide layer were formed on the surface due to the negative weight gain for Inconel 625, the weight loss is similar for the samples exposed to oxygen atmosphere and those in hydrogen atmosphere, -0.15 mg/cm^2 and -0.16 mg/cm^2. The weight loss can be a sign of metal degradation due to corrosion attack but without any oxide layer formed. A lack of oxide layer is an advantage with respect to contact resistance, since an oxide layer could higher the resistance and thereby lower the capacity of a fuel cell [7]. On the other hand a lack of oxide layer can be a problem respect to that no passivation occurs in terms of corrosion protection. Also, degradation of a metal in a fuel cell can cause problem with respect to an eventual diffusion of metal ions into the membrane. The conductivity of the membrane may then be lowered and thereby the efficiency of the fuel cell will be reduced [6]. The ICP-AES result shows that Inconel 625 has higher total leaching of ions than 316L and this strengthens the suggestion of degradation of Inconel 625 during exposure. It is difficult to predict if Inconel 625 would be more price worthy than 316L in a fuel cell, it needs to be investigated in an active fuel cell.

6. Conclusion

The exposure that is most oxidizing environment was the cathodic exposure at 180 °C and 25 % humidity, for one and three weeks. Longer exposure time and higher humidity gives a higher oxidation. The cathodic atmosphere is more corrosive than the anodic atmosphere and 316L coated with Max Phase is more resistant to corrosion than uncoated 316L.

The corrosion product is suggested to be amorphous $FeH_yP_2O_7$ for the cathodic exposures and partly crystalline $FeH_2P_2O_7$ for the anodic exposures. Nothing can be said about the amount of hydrogen for the cathodic corrosion product before further investigation.

Suitable methods for analysing the corrosion product are XRD and SEM with EDX. Good methods for quantification of oxidation are mass change and ICP atomic emission spectrometry. None of the resistance measurements methods was fine enough for quantification of the very localised oxidation on the samples.

Inconel 625 is more resistant to the formation of an oxide layer than 316L, but degradation of the metal occurs. It is difficult to draw a conclusion if Inconel 625 is better as metal for bipolar plates in fuel cell than stainless steel 316L.

7. Future outlook

Interesting for future work would be to do a cyclic furnace exposure where the temperature goes from room temperature up to 180 °C and down again, over and over again. This cyclic behaviour is to make a simulation of a realistic use of a fuel cell in a car and see if this environment results in a higher oxidation rate. There could also be of interest to investigate exposure at temperatures in between room temperature and 180 °C.

A future outlook would be to find a better method for measure the resistance, so the resistance can be used as a correct evaluation of the corrosion at the samples. A good method would be to use an apparatus that can measure many points of the samples at the same time and with the same pressure, an apparatus that can give reproducible results for all samples.

8. References

[1] A. Pozio, “Bipolar plate materials for PEMFCs: A conductivity and stability study,” Journal of power sources, vol. 179, pp. 631-639, 2008.

[2] Power Cell Sweden AB. (2012) Fuel Cells are part of the future clean power energy system. Power Cell Sweden AB. http://www.powercell.se/technology/bridge-to-the-future/. (2013-09-05)

[3] M. A. El-Sharkawi, Electrical Energy: An Introduction, 2nd ed., Boca Raton: CRC Press, 2009

[4] S. J. Andreasen. “Design and control of high temperature PEM fuel cell system,” Aalborg university, department of energy and technology, 2009.

[5] E. Otero, A. Pardo, M. V. Utrilla, E. Saenz, J. F. Alvarez, “Corrosion Behaviour of Aisi 293L and 205L Stainless Steels prepared by Powder Metallurgy in the Presence of Sulphuric and Phosphoric Acid,” Corrosion Sience, vol. 40, No. 8, pp. 1421-1434, 1998.

[6] F. Bruijn, G. J. Janssen, PEM Fuel Cell Materials: Costs, Performance and Durability. In: K-D. Kreuer, editors. Fuel Cells: Selected Entries from the Encyclopedia of Sustainability Science and Technology. New York: Springer Science + Business Media; 2013. p. 249-303.

[7] H. Ebrahimifar, M. Zandrahimi, “Influence of oxide scale thickness on electrical conductivity of coated AISI 430 steel for use as interconnect in solid oxide fuel cells,” International Journal of Ionics The Science and Technology of Ionic Motion, vol. 18, No. 6, pp. 615-624, 2012.

[8] G. G. Scherer, Fuel Cell Types and Their Electrochemistry. In: K-D. Kreuer, editors. Fuel Cells: Selected Entries from the Encyclopedia of Sustainability Science and Technology. New York: Springer Science + Business Media; 2013. p. 97-119.

[9] F. Barbir, PEM Fuel Cells, 2nd ed., Boston: Academic press, 2013.

[10] R. O´Hayre, S-W. CHA, W. Colella, F. B. Prinz, Fuel Cell Fundamentals, New Jersey: John Wiley & Sons Ltd., 2008.

[11] R. O´Hayre, D. M. Barnett, F. B. Prinz, “The Triple Phase Boundary: A Mathematical Model and Experimental Investigations for Fuel Cells,” Journal of The Electrochemical Society, vol. 152, pp. A439-A444, 2005.

[12] Z. Y. Chen, “The Role of Particles on Initial Atmospheric Corrosion of Copper and Zinc-Lateral Distribution, Secondary Spreading and CO2-/SO2-influence,” Stockholm: Royal Institute of Technology, 2005.

[13] R. Lindström, “On the Chemistry of Atmospheric Corrosion,” Göteborg: Chalmers reproservice AB, 2001.

[14] P. A. Schweitzer, Fundamentals of CORROSION, Mechanisms, Causes, and Preventative Methods, London: CRC Press Taylor & Francis Group, 2010.

[15] D. A. Jones, Principles and Prevention of Corrosion, New York: Prentice Hall, 1992.

[16] S. Syed, “Atmospheric Corrosion of Materials,” Emirates Journal for Engineering Research, vol. 11, pp 1-24, 2006.

[17] J. C. Riviere, S. Myhra, Handbook of Surface and Interface Analysis, Boca Raton: CRC Press Taylor & Francis Group, 2009.

[18] N. Birks, G. H. Meier, F. S. Pettit, Introduction to the high-temperature oxidation of metals, Cambridge: Cambridge University Press, 2006.

[19] F. P. Fehlner, M. J. Graham, Thin Oxide Film Formation on Metals. In: P. Marcus, editor. Corrosion Mechanisms in Theory and Practice. New York: CRC Press; 2002. p. 171-187.

[20] M. Zhanga, L. Guoqiang, W. Bo, S. Zhigang, "Composition optimization of arc ion plated CrNx films on 316L stainless steel as bipolar plates for polymer electrolyte membrane fuel cells," Journal of Power Sources, vol. 205, pp. 318–323, 2012.

[21] J. Pettersson, "Alkali Induced High Temperature Corrosion of Stainless Steel Experiences from Laboratory and Field," Göteborg: Svensk reproservice, 2008.

[22] P. Crook, "Corrosion of Nickel and Nickel-Base Alloys", ASM Handbook, Corrosion: Materials, vol. 13B, pp. 228-251, 2005.

[23] P. Eklund, M. Beckers, U. Jansson, H. Högberg, L. Hultman, "The Mn + 1AXn phases: Materials science and thin-film processing," Thin Solid Films, vol. 518, pp. 1851–1878, 2010.

[24] Department of Material Science and Engineering at Drexel University. (2013) MAX Phases. MAX Phase and AAC Research Groups. http://max.materials.drexel.edu/research-areas/max-phases/. (2013-07-11)

[25] D. Jürgens, M. Uhrmacher, H. Hofsäss, J. Röder, P. Wodniecki, A. Kulinska, M. Barsoum, "First PAC experiments in MAX-phases," Open Acess, vol. -, pp. -, 2008

[26] D. R. Gard. Phosphoric Acid and Phosphates. (2008) In Ullman´s Encyclopedia of Industrial Chemistry. http://onlinelibrary.wiley.com.proxy.lib.chalmers.se/ (2013-05-03).

[27] K. Schrödter, et al. Phosphoric Acid and Phosphates. (2005) In Kirk-Othmer Encyclopedia of Chemical Technology. http://onlinelibrary.wiley.com.proxy.lib.chalmers.se/ (2013-09-17).

[28] D. Stolten, B. Emonts, Fuel Cell Science and Engineering: Materials, Processes, Systems and Technology, Weinheim:Wiley VCH, 2012

[29] L. E. Smart, E. A. Moore, Solid State Chemistry: An Introduction, 3rd ed., Boca Raton: CRC Press, 2005.

[30] KU Leuven. (2012) X-ray diffraction – Bruker D8 Discover. KU Leuven. http://fys.kuleuven.be/iks/nvsf/experimental-facilities/x-ray-diffraction-2013-bruker-d8-discover]. (2013-06-10)

[31] E. K. L. Lerner, B. Wilmoth, "Scanning electron microscopy," World of Forensic Science, vol. 2, pp 598-599, 2005.

[32] J. G. Grolig, "Coated Ferritic Stainless Steels as Interconnects in Solid Oxide Fuel Cells," Göteborg: Chalmers reproservice, 2013.

[33] R. C. Dorf, J. A. Svoboda, Introduction to Electric Circuits, 6th ed., New York: John Wiley and Sons Inc., 2004.

[34] P. Atkins, L. Jones, Chemical Principles, The Quest for Insight, 4e ed., New York: W. H. Freeman and Company, 2008.

[35] D. C. Harris, Quantitative Chemical Analysis, 8e ed., China Lake: W. H. Freeman and Company, 2010.

[36] S-E. Mörtstedt, G. Hellsten, Data och diagram: Energi- och kemitekniska tabeller, 7th ed., Stockholm: Liber AB, 2008.

[37] K. R. Desai, Surface Chemistry, Jaipur: Global Media, 2008.

[38] F. Samavat, P. Taravati Ahmad, F. Mahmoodi , M. Faraz Samavat, M. Hossein Tavakoli, "The Effect of Annealing on the Size and Morphology of Palladium Nanoparticles," American Journal of Condensed Matter Physics, vol. 2, pp. 73–76, 2012.

[39] S. Molin, M. Gazda, B. Kusz, P. Jasinski, "Evaluation of 316 L porous stainless steel for SOFC support," Journal of the European Ceramic Society, vol. 29, pp. 757–762, 2009.